Coordination Chemistry Reviews 254 (2010) 2363–2390

Contents lists available at ScienceDirect

Coordination Chemistry Reviews

journal homepage: www.elsevier.com/locate/ccr

Review

Metal-containing nanofibers via coordination chemistry

Joseph K.-H. Hui, Mark J. MacLachlan*

Department of Chemistry, University of British Columbia, 2036 Main Mall, Vancouver, BC V6T 1Z1, Canada

Contents

ARTICLE INFO

Article history:
Received 13 November 2009
Accepted 9 February 2010
Available online 17 February 2010

Keywords:
Nanofibers
Electrostatic interactions
Supramolecular chemistry
Self-assembly

ABSTRACT

One-dimensional fibrous nanostructures may exhibit unique mechanical, optical, magnetic, and electronic properties as a result of their nanoscale dimensions. Various approaches have been used to prepare nanofibers (e.g., electrospinning, vapor deposition), but this review focuses on the research and development of self-assembled nanofibers formed through coordination chemistry. By employing metal–ligand interactions that extend along the backbone of the aggregates, nanofibrous, often gel-forming, materials with appealing properties have been formed. Other fibers formed through electrostatic interactions between charged coordination complexes are also discussed. The optical, electronic, and magnetic properties conferred upon the materials by the embedded coordination complexes render the nanofibers useful for applications in the fields of catalysis, sensors, and gas storage, and potentially for developing nanosized devices.

1. Introduction

The field of nanochemistry is rapidly expanding, and will lead to facile routes to construct sophisticated nanoscale materials [1]. This "bottom-up" approach has many benefits over traditional "top-down" approaches (e.g., lithography) as it enables more control of the molecular architecture and assembly of more sophisticated structures. Over the past several decades, supramolecular self-assembly has emerged as a powerful technique for the construction of complicated, often hierarchical materials with significant functions and properties. The utility of supramolecular chemistry in the construction of nanomaterials and devices is well-exemplified by recent work in the literature, including the one-pot, 18-component assembly of diformylpyridine, 2,2′-bipyridine-containing diamine and zinc ions into three macrocycles that interlock into the shape of a Borromean ring [2], the self-assembly of tris-2,2′-bipyridine and iron(II) chloride into a circular double helicate [3], conjugated polyrotaxanes composed of cyclodextrin with threads based on poly(*para*-phenylene), polyfluorene, and poly(diphenylenevinylene) and stoppered with naphthalene groups [4], and the family of metal–organic frameworks with metal–oxygen polyhedra linked by bridging ligands [5].

The applications of nanostructured supramolecular assemblies depend on the shapes and their functionalities, which can be imparted by selection of molecular precursors. For instance, bowl-shaped complexes can self-organize into nanocapsules for host–guest chemistry [6] and structures shaped like badminton shuttlecocks can organize into one-dimensional columnar structures [7]. By choosing precursors with specific geometries,

* Corresponding author.
E-mail address: mmaclach@chem.ubc.ca (M.J. MacLachlan).

0010-8545/$ – see front matter © 2010 Elsevier B.V. All rights reserved.
doi:10.1016/j.ccr.2010.02.011

nanostructures with particular forms may be anticipated. However, it is often by chance that new nanomaterials are discovered, and their shapes may not be obvious extensions of the molecular geometry.

Nanofibers are an exciting class of materials with excellent potential for real applications, fundamental investigations, and for understanding biological systems. They are long-range-ordered, one-dimensional, nanosized supramolecular aggregates that can be linear or helical [8]. Nanofibers have been investigated in nanosized electronic [9], mechanical [10] and medical fields [11]. One-dimensional nanostructures are also ubiquitous in biological systems, exemplified by collagen, axons, and keratin. There has been a rapid growth of interest in generating biomimetic fibrous structures with medical applications in terms of compatibility, degradability and cell–matrix interactions [12].

One interesting property that is frequently observed for nanofibers is gelation. The fibers form network structures, often through weak interfiber interactions, that can trap and immobilize solvent molecules, resulting in the formation of a gel [13]. Gels are interesting materials and already have a wide range of applications including biomedical applications [14], drug delivery [15], and catalysis [16], depending on the nature of the materials forming the nanofibrils. They are also being explored for environmental sensors and have been used to template sol–gel polycondensation of metal alkoxides such as tetraethyl orthosilicate (TEOS) and tetra-*n*-butyl titanate [17]. Given their interesting applications and properties, the synthesis and investigation of nanofibers with unique properties has become an attractive topic for researchers [18].

Numerous methods have been employed to manufacture nanofibers that span diverse size ranges. One way to produce fibrous nanostructures artificially is through the electrospinning technique. This process involves applying a high voltage between a metal collector plate (generally rotating) and the tip of a tiny needle that is ejecting a viscous polymer solution [19]. The polymer solution becomes charged in the electrical field, inducing electrostatic repulsion that creates a charged jet of solution erupting from the tip of the needle. While the jet is in air, the solution evaporates and the nanofibers deposit on the metal collector [20]. This method has many advantages – it allows good control over the morphology and porosity of the fibers, and it can be applied to diverse polymers and mixtures, permitting good control over composition [21]. The diameters of the electrospun fibers are in the range of nanometers to micrometers, but their lengths can extend to the kilometer scale [22]. These synthetic polymeric fibers possess good physical properties, including high specific surface area, flexibility in surface functionalities, and superior mechanical properties, which impart the nanofibers with excellent properties for use in biomedical engineering [21]. Long hollow nanofibers can also be fabricated by electrospinning [23], thus enhancing the specific surface area. Complementary to electrospinning, supramolecular self-assembly has also received a great deal of attention for making nanofibers. Appropriately designed molecules and macromolecules act as the building units of the fibrillar aggregates, which then assemble into one-dimensional nanostructures through non-covalent interactions, such as hydrogen-bonding, intermolecular π–π stacking, electrostatic interaction/coordination chemistry, or the hydrophobic effect [24]. These molecule-based construction approaches to nanofibers provide a way to diversify the properties of the aggregates by tuning the functionalities of the building units. In recent years, fabrication of one-dimensional nanostructures has predominately involved intermolecular hydrogen-bonding and π–π stacking, or a combination of both non-covalent interactions, but significantly fewer with metal–ligand coordination interactions. Nevertheless, coordination chemistry offers a large and fascinating assortment of complexes with different geometries, and electronic and magnetic properties that can be incorporated into nanomaterials. Indeed, many elegant inorganic nanostructures with well-defined shapes, such as helicates, nanoboxes, catenanes and nanocages [25], have been built using coordination chemistry, often relying on the bonding angles and geometry at the metal centers to dictate the final structure. Nanofibers constructed from extensive one-dimensional metal–ligand coordination interactions are an appealing class of materials because of their potential applications including catalysis, sensing, and gas storage. Their interesting electronic and magnetic properties also make them good candidates for nanoscale devices [26]. One can imagine using changes at the metal center (e.g., changes in coordination number, oxidation state, or electronic configuration) as a means to change the properties of the material.

In this review, we describe the use of coordination chemistry to obtain nanofibers. In some cases, the assembly is formed through electrostatic interactions rather than extended metal–ligand interactions, but all contain metals and the metal is important to the assembly. We have restricted the review to examples where the fiber morphology has been imaged by a technique such as transmission electron microscopy (TEM), scanning electron microscopy (SEM), or atomic force microscopy (AFM). We also do not include the vast number of rigid nanocrystallites that can resemble fibers. We have primarily covered recent exciting developments in the field, and there are undoubtedly other reported examples of nanofibers from coordination complexes (some of these are described in Section 4).

2. Nanofibers constructed from macrocyclic units

Numerous types of macrocycles have been synthesized and studied, and they have played an important role in the development of the field of supramolecular chemistry. Some well-known groups of macrocycles, including crown ethers, aza-crowns, cryptands and cyclodextrins, are capable of coordinating to metal ions within their cavities [27], which provide insight into supramolecular interactions and molecular recognition. The metal-containing macrocycles can exhibit intriguing magnetic, catalytic, or supramolecular behavior [28]. There are several reports of using intermolecular hydrogen-bonding and π–π stacking as the driving forces of aggregation to form self-assembled fibrous superstructures from macrocycles [29]. Another approach to fabricate one-dimensional nanofibers is by using the metal–ligand coordination or electrostatic interactions. With macrocycle-based examples, most of these use the latter, where the charge of the metal complex is central to the assembly.

2.1. Metalloporphyrins and metallophthalocyanines

Porphyrins are shape-persistent and conjugated macrocycles comprised of four pyrrole subunits that are interconnected by methine bridges. These heterocycles can be used as proligands to coordinate various metals in their central cavities; metallated porphyrins play important roles in nature, such as in heme and chlorophyll. The π-conjugated backbone, the metal center and the functional groups appended on the periphery render the metalloporphyrins the ability to self-assemble into a variety of supramolecular structures through non-covalent interactions [30]. Extensive efforts have been devoted to the research of multiporphyrin arrays due to their promising applications in molecular switching, electronic and photonic devices [31]. Intermolecular π–π stacking and hydrogen-bonding are commonly used to induce nanofiber structures [32]; these interactions can also combine with coordination chemistry and electrostatic interactions to construct beautiful fibrous networks and to prepare excellent gelators [33]. One-dimensional polymeric metalloporphyrins synthesized solely

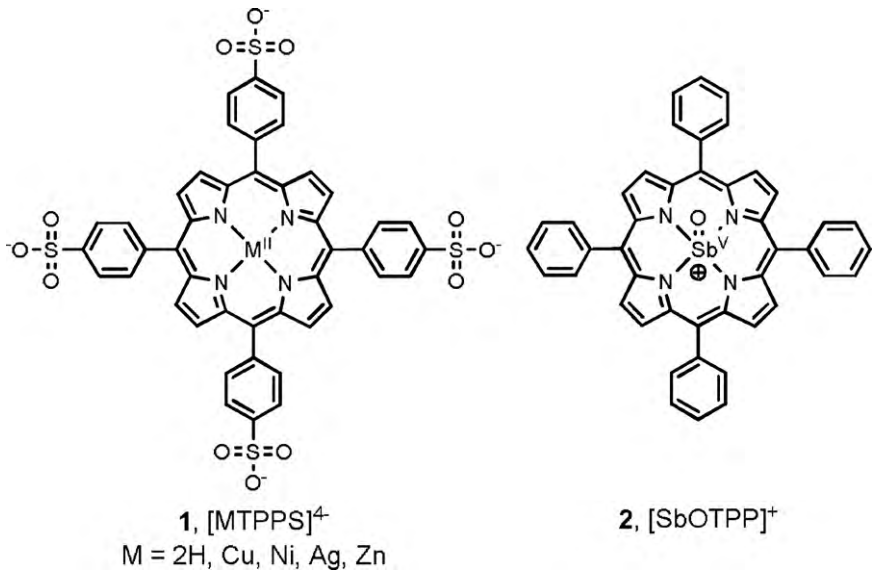

Fig. 1. Chemical structures of porphyrins **1** and **2**.

by coordination chemistry and electrostatic interactions have been observed in solution and in the solid state [34]. Shelnutt and co-workers reported the formation of porphyrin nanotubes through the self-assembly of two oppositely charged porphyrins in aqueous solution [35]. The nanotubes can be used as photocatalysts to reduce metal complexes and deposit the metals onto the surfaces of the nanotubes, thus forming nanoscale metal–composite structures. This ionic self-assembly approach provides the ability to alter the molecular building subunits in order to control the structural and functional properties of the nanostructures. Shelnutt and co-workers also demonstrated a phase transfer ionic self-assembly approach to obtain bundles of porphyrin nanofibers employing water-soluble porphyrins (**1**, $[MTPPS]^{4-}$) and water-insoluble oxo-antimony(V) porphyrin (**2**, $[SbOTPP]^{+}$) (Fig. 1) in an aqueous/dichloromethane mixture [36]. The bundles of nanofibers are 70–140 nm wide and 1–2 μm long, with each individual fiber having a diameter of 20–40 nm (Fig. 2). Photocatalytic studies showed that these porphyrin nanofiber bundles can reduce metal complexes and attain metal clusters (10–100 nm in diameter, depending on the metal center of porphyrin **1**) on the surface of the nanofibers. The photoactivity of these bundles directly takes advantage of the intrinsic properties of the inorganic building blocks and demonstrates that the preparation of porphyrin–metal composite nanostructures can lead to potential applications in electronics and photonics.

Taking advantage of metal–ligand coordination interactions, chemists have produced one-dimensional polymeric metalloporphyrin aggregates. Shinkai and co-workers reported a porphyrin with eight pyridyl groups (**3**) that self-assembles into a coordination polymer (**4**) through Pd(II)-pyridine interactions with four *cis*-Pd(II) complexes (Scheme 1) [37]. A light-scattering study of a chloroform solution of porphyrin polymer **4** revealed that the aggregate is assembled in solution, but the polymeric structure was not observed in polar solvents (e.g., in a mixture of 7:3 (v/v) chloroform/methanol). From these results, the authors concluded that the stability of the Pd(II)-pyridine coordination bonds is influenced by the solvent, which directly affects the occurrence of the porphyrin polymeric structure and allows one to use solvent to control the assembly. When a chloroform solution of polymer **4** was dried and viewed under TEM, long nanofibers with diameters of ca. 10 nm were observed (Fig. 3). It is noteworthy that the theoretical structure of porphyrin polymer **4** shown in Scheme 1

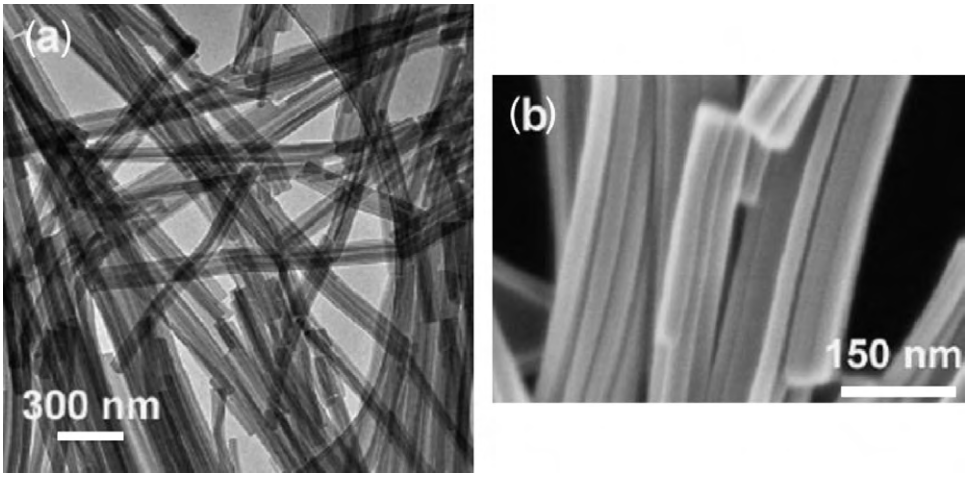

Fig. 2. (a) TEM and (b) SEM images of the bundles of porphyrin nanofibers.

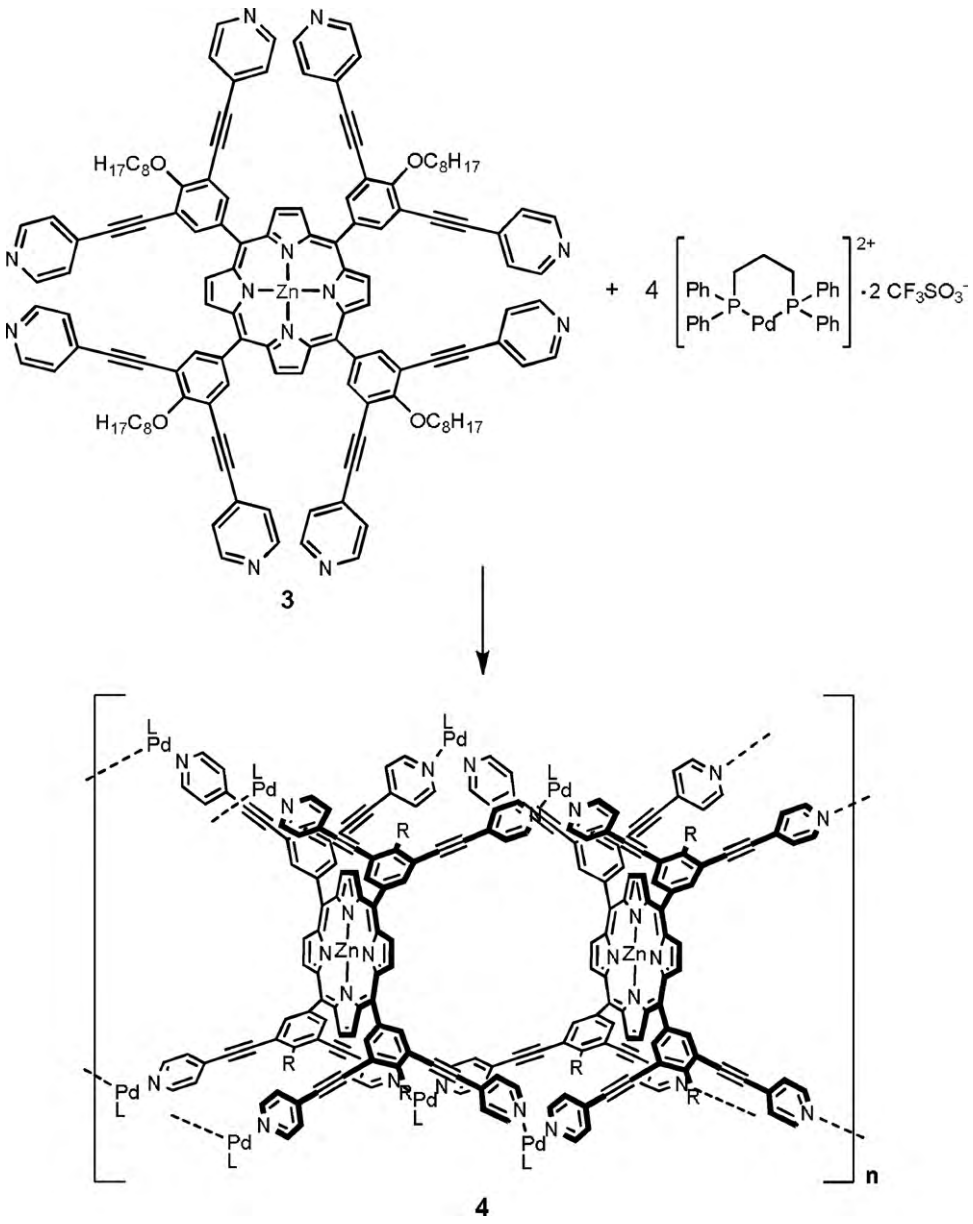

Scheme 1. Synthesis of porphyrin coordination polymer **4**.

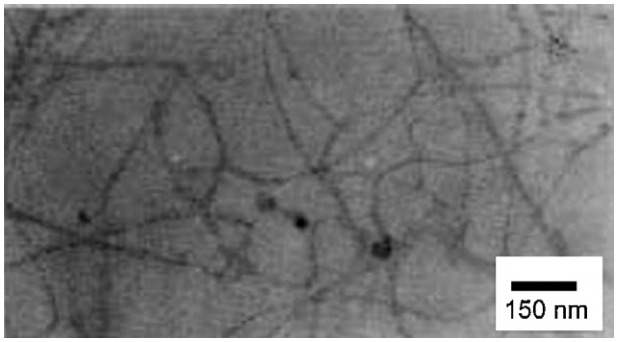

Fig. 3. TEM image of the porphyrin nanofibers.
Copyright 2001 The Chemical Society of Japan. Reproduced with permission from ref. [37].

possesses many large cavities. As a result of these cavities, the polymer can bind guest molecules such as 4,4′-trimethylenedipyridine, in which each of the two pyridyl units coordinates to the axial position of different Zn(II) centers and bridge two porphyrin planes. The inclusion of various guest molecules in the cavities of the polymeric structure, where they can interact with the metal and the π-conjugated system, can potentially tune the properties of the porphyrin nanofibers.

Phthalocyanines are chemical cousins of porphyrins – related, but different – that have received attention due to their optical, catalytic, electronic, photonic, and chemical sensing properties [38]. Phthalocyanines are generally easier to prepare than porphyrins, and this has helped them to flourish. Like porphyrins, phthalocyanines are capable of assembling into one-dimensional supramolecular structures through non-covalent intermolecular interactions. Many polymeric superstructures have been prepared and analyzed in solution. Tung and co-workers reported the preparation of Zn(II)-containing phthalocyanines with four aryloxy substituents (**5a** and **5b**, Fig. 4) [39]. In solution, J-aggregates

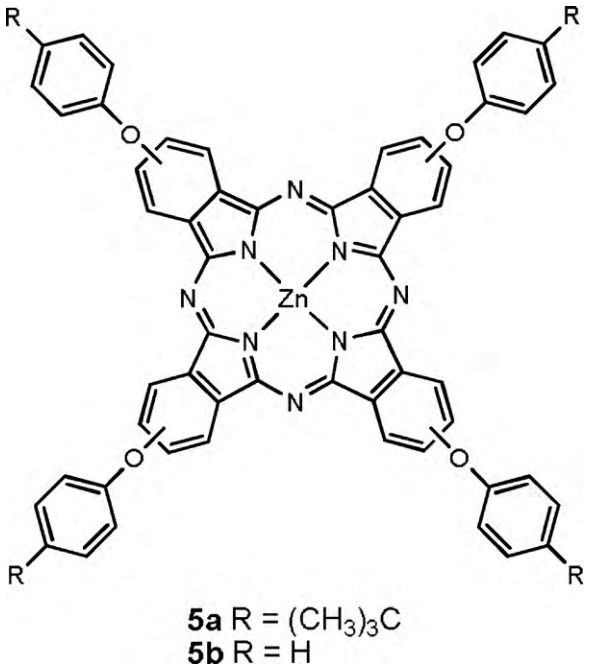

Fig. 4. Chemical structure of phthalocyanines **5a** and **5b**.

were observed by UV–visible spectroscopy in non-coordinating solvents and this was supported by the red-shifted and split Q-bands when compared to the absorption spectra of monomeric Zn(II)-containing phthalocyanines in coordinating solvents. The J-aggregation of **5a** and **5b** in non-coordinating solvents was also confirmed by matrix-assisted laser desorption ionization time-of-flight (MALDI-TOF) mass spectrometry. A mass spectrum of **5a** prepared from a chloroform solution showed eight distinct peaks corresponding to monomer and oligomers (up to octamer), consistent with aggregation. In addition, the aggregates were studied with TEM, imaging samples of **5a** deposited from chloroform. The TEM micrograph, shown in Fig. 5a, depicts a two-dimensional network structure constructed from nanofibers about 50 nm in diameter. When the sample for TEM was prepared at a lower concentration, nanoparticles were observed along with the network (Fig. 5b). The authors proposed that the aggregation of these complexes is mediated by Zn···O interactions, where the ether oxygen in the aryloxy group of one phthalocyanine molecule can coordinate to the Zn(II) center of the neighboring phthalocyanine molecule. This is substantiated by control experiments that disrupted the aggregation by coordinating solvents. For example, the addition of coordinating solvent during the TEM sample preparation disrupted the Zn···O interactions and, as a result, no network structure was detected.

Würthner and co-workers took advantage of the Zn···O interactions, along with intermolecular hydrogen-bonding and π–π interactions, to obtain tubular J-aggregates from a series of Zn(II) chlorins (one of the porphyrin analogues) in aqueous and organic media [40]. These self-assembled Zn(II) chlorin structures that mimic the supramolecular organization of natural light harvesting systems (e.g., bacteriochlorophylls) form well-defined short nanorods (lengths of ca. 300 nm and heights of ca. 6 nm) rather than extended nanofibers observed in the other structures discussed.

Although most fibers have been constructed from aggregates that form in solution, fabrication of supramolecular assemblies using a liquid–liquid interface has drawn some attention. Mg(II)-containing phthalocyanines with eight chiral thioether substituents on the periphery ($MgPc(SEtPh)_8$, **6**) were synthesized by Watarai and co-workers (Fig. 6) [41]. These phthalocyanines can bind Pd(II) ions to their peripheral sulfur atoms and exhibit two different modes of aggregation in toluene and at the toluene/water interface. When $PdCl_2$ was introduced to $MgPc(SEtPh)_8$ in toluene, two phthalocyanine molecules stack into an H-type dimer in a twisted fashion with four Pd(II) centers acting as the bridges between the phthalocyanine planes. These twisted H-type dimers of (*R*)- and (*S*)-$MgPc(SEtPh)_8$-Pd(II) complexes could be detected by blue-shifted Q-bands in UV–visible absorption spectra and Cotton effects in circular dichroism (CD). In contrast to the twisted dimers obtained in toluene, one-dimensional helical J-aggregation was observed when $MgPc(SEtPh)_8$ was combined with $PdCl_2$ at the toluene/water interface. UV–visible spectra of the $MgPc(SEtPh)_8$-Pd(II) complexes showed that the Q-bands were red-shifted and CD spectra displayed Cotton effects for both complexes. These absorption and CD spectral data indicated that the interfacial J-aggregates of (*R*)- and (*S*)-$MgPc(SEtPh)_8$-Pd(II) complexes are oriented in left-handed and right-handed helical arrangements, respectively. The models of the helical J-aggregates are depicted in Fig. 7a. Field emission (FE) SEM images of the dried sample of Pd(II)-induced supramolecular structures revealed fibrous networks (Fig. 7b and c) in which the individual fibers are ca. 80–120 nm in width and over 500 nm in length. Moreover, twisted fibers could be seen by FE-SEM (Fig. 7c), supporting the CD spectral data showing helical arrangements of the interfacial J-aggregates. Watarai and co-workers also reported the toluene/water interfacial method to fabricate nanorods and nanoribbons that are facilitated by other thioether-derivatized Mg(II)-containing phthalocyanines and Pd(II) complexes [42]. It is noteworthy that the self-assembled superstructure can be controlled by combining the building units in a single liquid medium or at the interface of two immiscible liquids.

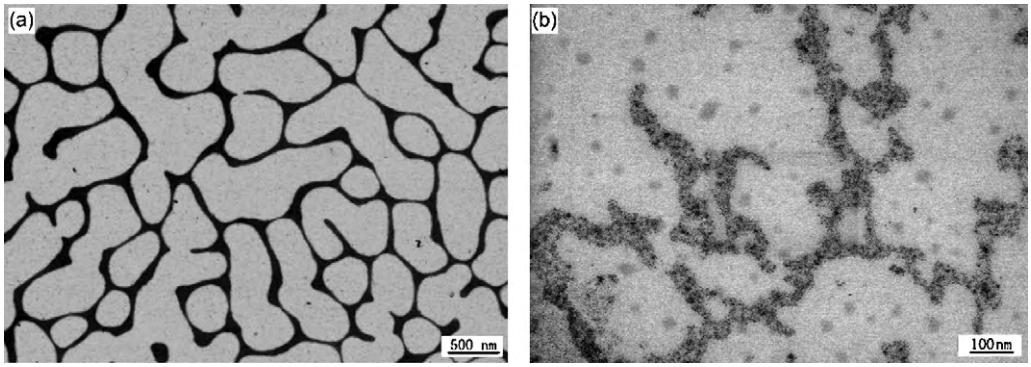

Fig. 5. TEM images of samples of **5a** prepared from chloroform at concentrations of (a) 1×10^{-5} M and (b) 1×10^{-6} M.

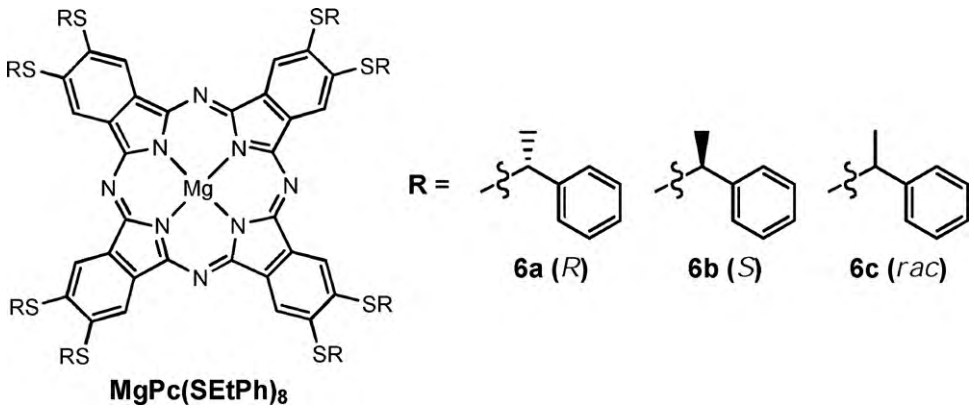

Fig. 6. Chemical structures of $MgPc(SEtPh)_8$ complexes **6a**–**6c**.

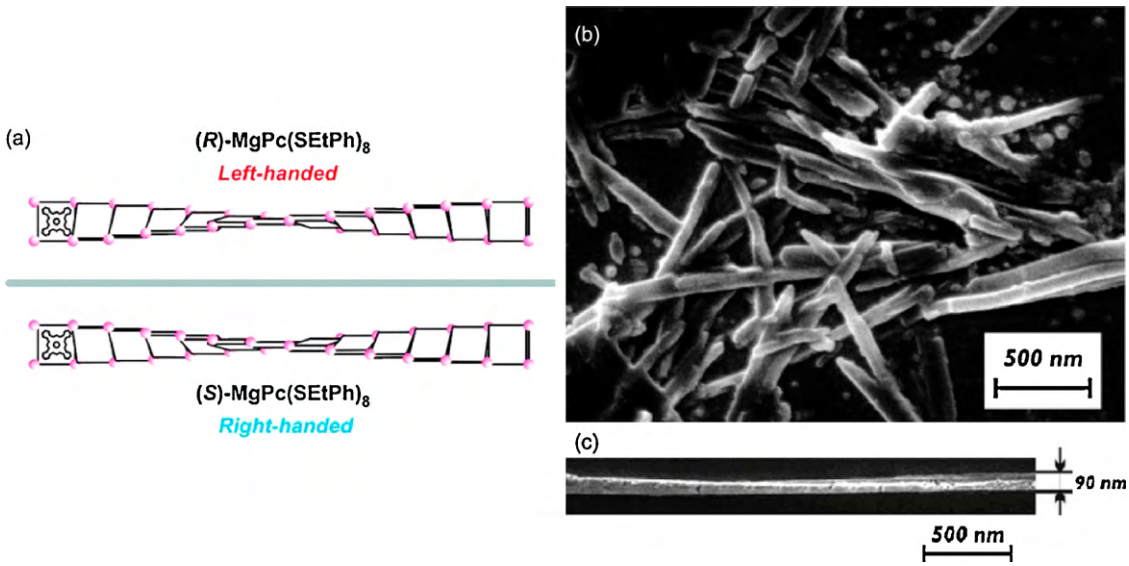

Fig. 7. (a) Schematic representation of the helical arrangement of the interfacial J-aggregate of $MgPc(SEtPh)_8$-Pd(II) polymeric structure ($MgPc(SEtPh)_8$ = squares, $PdCl_2$ = spheres). FE-SEM images of the interfacial aggregate of (b) (*R*)-$MgPc(SEtPh)_8$-Pd(II) and (c) (*S*)-$MgPc(SEtPh)_8$-Pd(II) complexes. Twisted fibers can be clearly seen in (c).

2.2. Ion-induced self-assembly

Macrocycles with large interior pores and appropriate functionality are anticipated to accommodate one or more guest molecules. Crown ethers, for example, are well-known to selectively bind cations to form metal complexes. Occasionally, the inclusion of guest metal ions in a macrocycle can lead to the formation of supramolecular architectures. Lehn and co-workers obtained nanofibers from macrocycle **7** (Fig. 8) through K^+ ion-induced assembly [43]. The central cavity of macrocycle **7**, which has three 1,8-naphthyridine groups with the lone pairs on the nitrogen atoms directed inwards, resembles that of an aza-crown and thus was expected to bind K^+ ions in solution (Fig. 9a). Upon addition of potassium picrate to macrocycle **7** in chloroform-d_1/methanol-d_4, the authors detected aggregation by ^1H NMR spectroscopy through broadening and shielding of the proton signals. The solid-state structure of the assembly was investigated by a TEM study of a dried sample of macrocycle **7** with K^+ ions. When deposited from a chloroform/nitromethane mixture, fibers about 50 nm in diameter and microns in length were observed (Fig. 9b). This aggregation approach promoted by alkali metal ions can also be observed in other macrocyclic systems [24f,44].

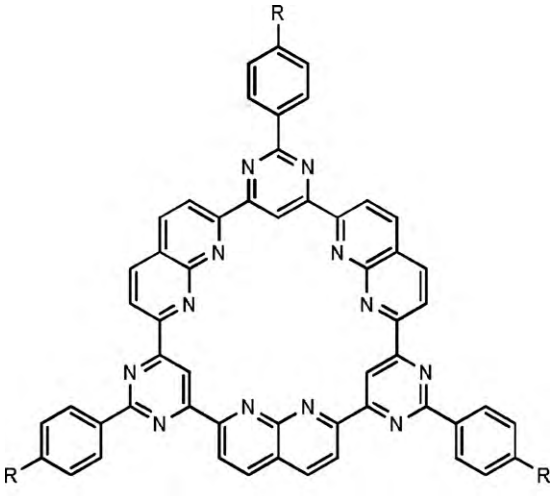

Fig. 8. Chemical structure of macrocycle **7**.

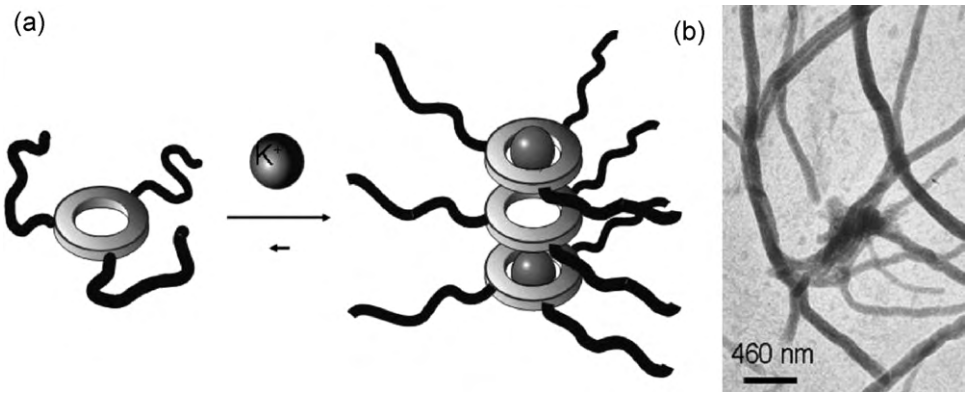

Fig. 9. (a) Schematic representation of the presumed aggregation process of macrocycle **7** with K^+ ions. (b) TEM image of macrocycle **7b** with K^+ prepared in chloroform/nitromethane.

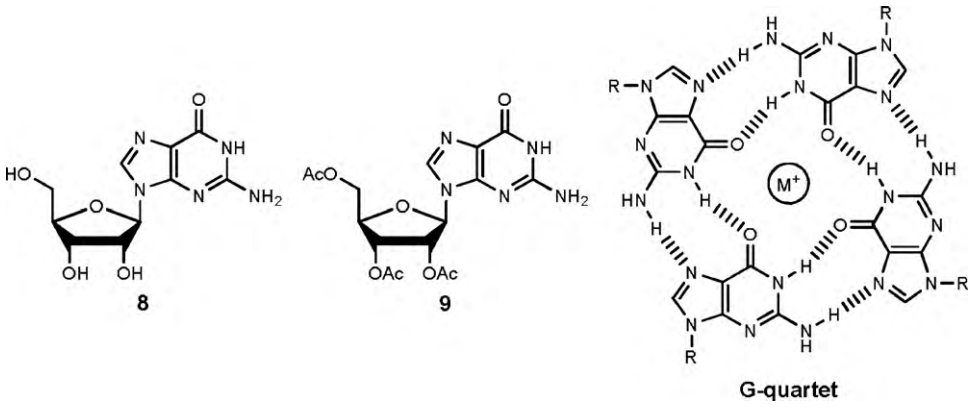

Fig. 10. Chemical structures of guanosines **8** and **9**, and a G-quartet.

In nature, one can find many exquisite examples of self-assembly to inspire chemists in designing complex macromolecular assemblies and bio-inorganic composite materials. Biomolecules are often used utilized as constituents for studying biomimetic supramolecular assembly, and their organization can be facilitated by alkali cations. For instance, guanosine, a nucleoside comprising guanine attached to a ribose ring, can associate into macrocyclic tetramers (G-quartets) through hydrogen-bonding in the presence of alkali metal ions such as Na^+ and K^+. The G-quartets can further self-assemble into columns with the cations being sandwiched between the layers of G-quartets [44b, c,45]. Davis and co-workers reported the synthesis of calix[4]arene appended with four guanosine substituents and took advantage of the tendency of the ion-assisted self-assembly of guanosine in which tubular structures were obtained upon the addition of $NaBPh_4$ [46]. The Na^+ ions are located at the inner core of the cation-filled channels and the

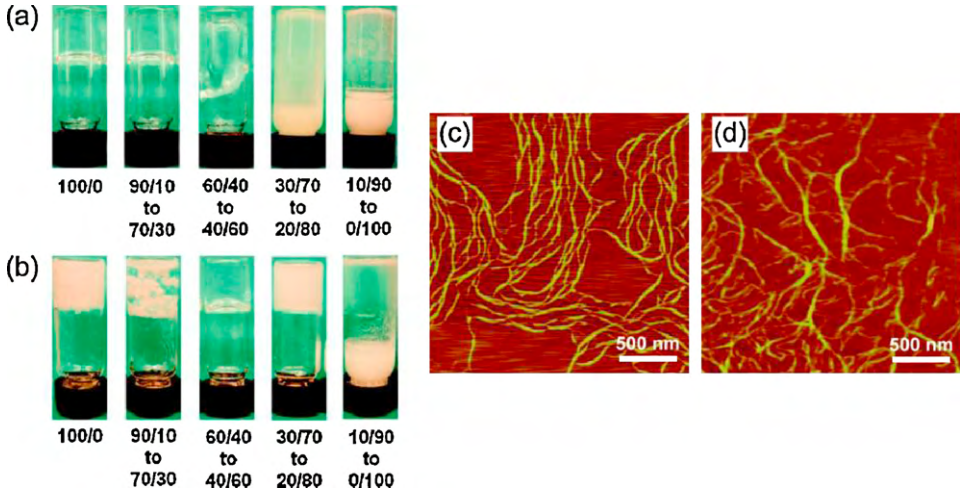

Fig. 11. Visual appearance of the hydrogels obtained from guanosine **8** and guanosine **9** in aqueous potassium chloride solution (a) 15 min and (b) 36 h after sample preparations. The ratios are listed as guanosine **8**/guanosine **9**. (c and d) AFM images of the 60/40 and 40/60 gels, respectively.

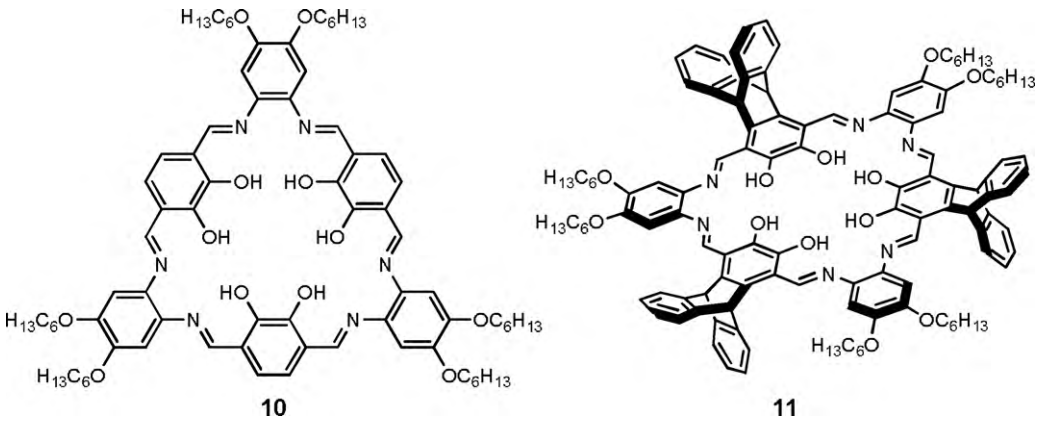

Fig. 12. Chemical structures of Schiff base macrocycles **10** and **11**.

nanotubes could be seen by TEM. However, it was the intermolecular hydrogen-bonding of two guanosine units of one calix[4]arene molecule with two of the neighboring guanosine units to form the G-quartets that led to the tubular aggregation. Rowan and coworkers reported the formation of hydrogels from a mixture of guanosines **8** and **9** (Fig. 10) in aqueous potassium chloride [47]. The G-quartets generated in this case would be random hydrogen-bonding combinations between the two guanosines. Guanosine **8** can gelatinize in the presence of sodium or ammonium salts, but the resulting hydrogel showed poor stability (collapse of gel occurred after a short period of time at room temperature) [48]. It was found that the introduction of hydrophobic non-gelling guanosine **9** to guanosine **8** increased the stability of the hydrogel due to the hydrophobic groups of guanosine **9** promoting cross-linking between the columnar stacks. In addition, the physical appearance and the stability of the gel can be tuned by varying the ratio of the two guanosines (guanosine **8**/guanosine **9**) in the gelation process (Fig. 11a and b). Based upon the stability of the hydrogels, the ratios in the range of 60/40 to 40/60 of guanosine **8**/guanosine **9** are the most effective combinations to prevent the gels from collapsing (even after a year at room temperature). AFM studies were performed on the dried 60/40 and 40/60 gel samples in order to characterize the assembled networks. The micrographs showed nanofibers in both gel samples, but the morphology differs slightly with respect to the ratio of the two guanosine units (Fig. 11c and d). The fibers of the 40/60 gel are shorter and wider than those of the 60/40 sample. The increase in fiber width is ascribed to more cross-linking between the fibrillar guanosine stacks driven by the hydrophobic effect that was enhanced by the addition of guanosine **9**. In addition, the length of the fibers decreased with increasing guanosine **9** content because the stacking of the guanosine units was disrupted by the acetyl groups of guanosine **9**.

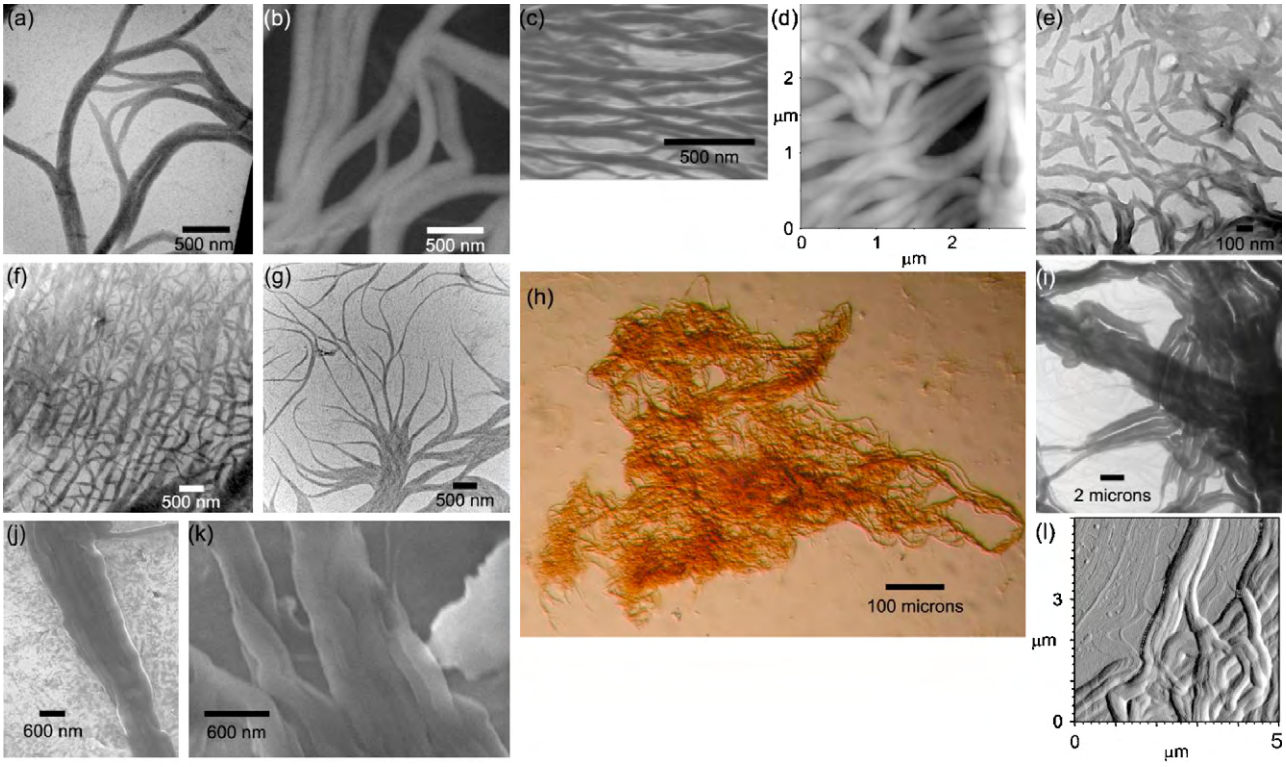

Fig. 13. (a and b) TEM, (c) SEM, and (d) AFM micrographs of [Na·**10**]BF_4. (e) TEM image of macrocycle **10** with $NaBPh_4$. (f) TEM of [Na·**10**]BF_4 dried in 10 s at 92 °C and (g) 80–90 min at room temperature. (h) Optical, (i) TEM, (j and k) SEM, and (l) AFM (amplitude trace) micrographs of macrocycle **10** with NH_4BF_4.

Guanine-rich DNA segments have also been shown to assemble into extended structures with embedded ion channels through alkali- and alkaline-earth metal ion assembly [49]. This research in biological self-assembly may help to design new biosensors, and to improve our understanding of ion transport in nature.

MacLachlan and co-workers applied a similar approach to construct hierarchical nanofibers in the presence of alkali metal and ammonium salts from Schiff base macrocycle **10** (Fig. 12) [50]. Macrocycle **10** is a conjugated molecule that has a central pore resembling 18-crown-6 in the hexagonal arrangement of the hydroxyl groups. In contrast to crown ethers, however, the rigid backbone of the macrocycle prohibits it from contorting sufficiently to offer an adequate binding site for Na^+. Addition of $NaBPh_4$ and other alkali metal tetraphenylborate salts to macrocycle **10** gave spectroscopic evidence for aggregation in solution [51]. NMR titrations in particular showed that the macrocycles were stacked on top of one another in the aggregated state. When a chloroform solution of macrocycle **10** was treated with $NaBF_4$, a color change from orange to deep red was observed. The sodium ion binds to the interior of the macrocycle and is accompanied by an uncoordinated counteranion, BF_4^-. The solution of [Na·**10**]BF_4 was cast on a solid substrate and the morphology was studied by TEM, SEM and AFM (Fig. 13a–d). TEM showed nanofibers with diameters of ca. 170 nm (Fig. 13a and b), considerably larger than the diameter of macrocycle **10** (ca. 2–3 nm). SEM also revealed the fiber morphology in the sample (Fig. 13c) and the bundles appear cylindrical in shape. AFM in tapping mode showed that the samples are relatively smooth and approximately the same size as observed by TEM (Fig. 13d). Macrocycle **10** binds Na^+ in its interior to form a highly charged polymer, where alkali metals are coordinated by the macrocycles through Na···O interactions. These polyelectrolytic aggregates further condense into much larger nanofibrillar bundles through electrostatic interactions between the anions and the polyelectrolyte. The positions of the Na^+ and BF_4^- were confirmed by solid-state NMR spectroscopy, which showed relatively fast relaxation for the anion (located outside of the tube) and slow relaxation of the cation (pinned inside the tube). Since the formation of the one-dimensional fibrous structure is ascribed to the macrocycles being bridged by the Na^+ ions, the introduction of bulky substituents should block the supramolecular assembly. Macrocycle **11** with triptycenyl substituents (Fig. 12) was prepared. In the case of macrocycle **11**, the bulky triptycenyl groups prevented columnar assembly and, therefore, no fibrous structure was observed. The morphology and size of the fibrous superstructure could be tuned by the choice of salts and evaporation time. For instance, when larger anions were employed (e.g., BPh_4^-), the fibers obtained were short and poorly defined (Fig. 13e). Moreover, short nanofibers were also obtained with rapid evaporation (Fig. 13f), whereas very long, well-organized fibers were generated with a slow evaporation rate (Fig. 13g). It is noteworthy that when NH_4BF_4 was combined with macrocycle **10**, an additional level of hierarchy in the fiber morphology could be observed. Similar to Na^+, one-dimensional polymeric structures were formed with the NH_4^+ cations hydrogen-bonded in the interior of the macrocycles. The nanofibers further assembled into bundles with diameters of hundreds of microns and lengths of millimeters (Fig. 13h–l). Nanofibers with diameters of ca. 200 nm were observed by TEM (Fig. 13i). This feature could also be seen clearly by SEM (Fig. 13j and k) and AFM (Fig. 13l). The supramolecular self-assembly underwent a four-level hierarchy that spanned six orders of magnitude in length (from nm to

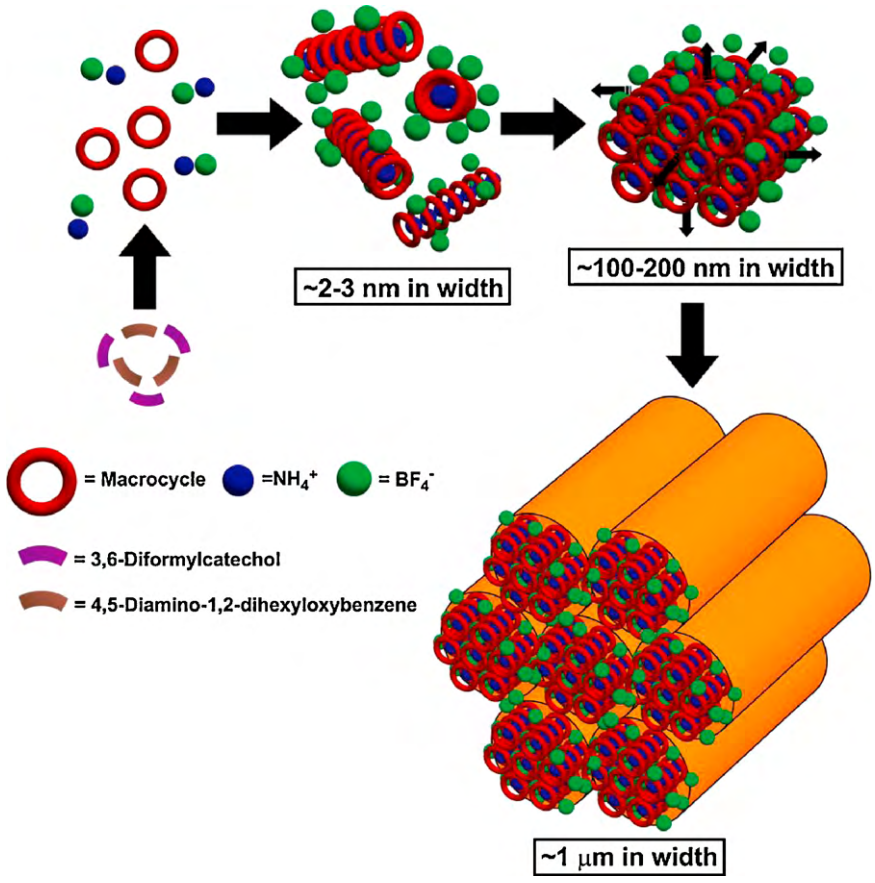

Fig. 14. A graphic representation of the four-level hierarchical assembly.

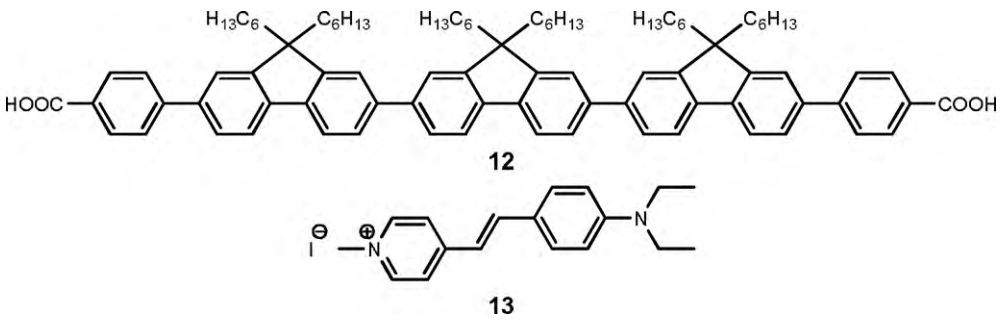

Fig. 15. Chemical structures of π-conjugated donor **12** and acceptor **13**.

mm) whereby the precursors to macrocycle **10** (dimensions of ca. 0.5 nm) reacted to form macrocycle **10** (diameter of ca. 2–3 nm), which assembled into a polyelectrolytic assembly, then further organized into nanofibers and microfibers (Fig. 14).

3. Nanofibers obtained from coordination polymers

Supramolecular self-assembly of molecules and macromolecules into one-dimensional polymeric structures through coordination chemistry or electrostatic interactions has been a quest for many researchers. The coordination polymers are reversible aggregates that can break and reconnect during reactions, facilitating self-assembly. The use of the concept of extended metal–ligand interaction to construct fibrous nanostructures provides a way to diversify the properties of the assemblies by tailoring the functionalities of the organic ligands and varying the choice of metal centers. Nanofibers have also been imaged in some metal-containing gels [52]. There have been several reports of generating fibrous materials and networks with coordination polymers, and examples of these will be discussed later in this section.

3.1. Metal–ligand coordination

Nanofibers constructed from metal ions and organic bridging ligands into coordination polymers have been research targets of interest because they can be simple to synthesize, but offer plentiful opportunities for structural variation and potential access to useful properties. For instance, Loh and co-workers designed and obtained a one-dimensional nanostructured light-harvesting antenna that can transform UV to red radiation [53]. The coordination-assisted self-assembly of the nanostructure involves the strong affinity between the two carboxylate groups of π-conjugated donor **12** (Fig. 15) and Zn(II) ions in the presence of acceptor **13** (Fig. 15). TEM and SEM studies of the assembled structure showed that nanofibers were obtained (Fig. 16a and b, respectively) and they have diameters of 20–30 nm and lengths of up to several microns. The metal–ligand interactions of donor **12** and Zn(II) ions, accompanied

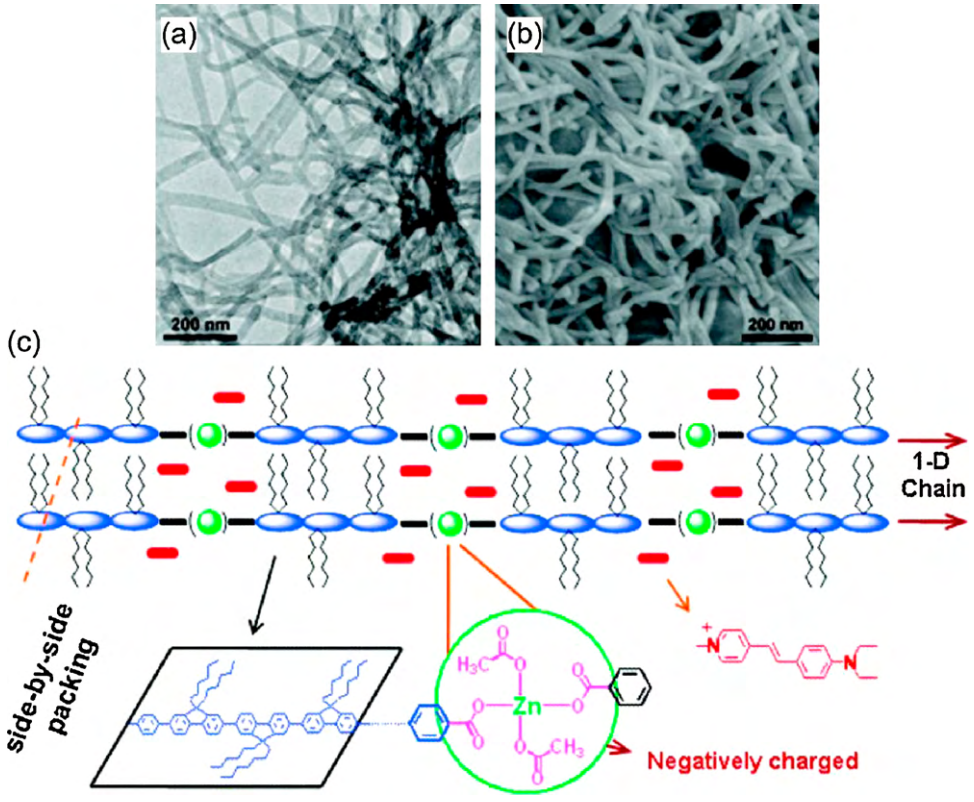

Fig. 16. (a) TEM and (b) SEM images of the nanofibers. (c) Schematic representation of the coordination-assisted self-assembly mechanism.

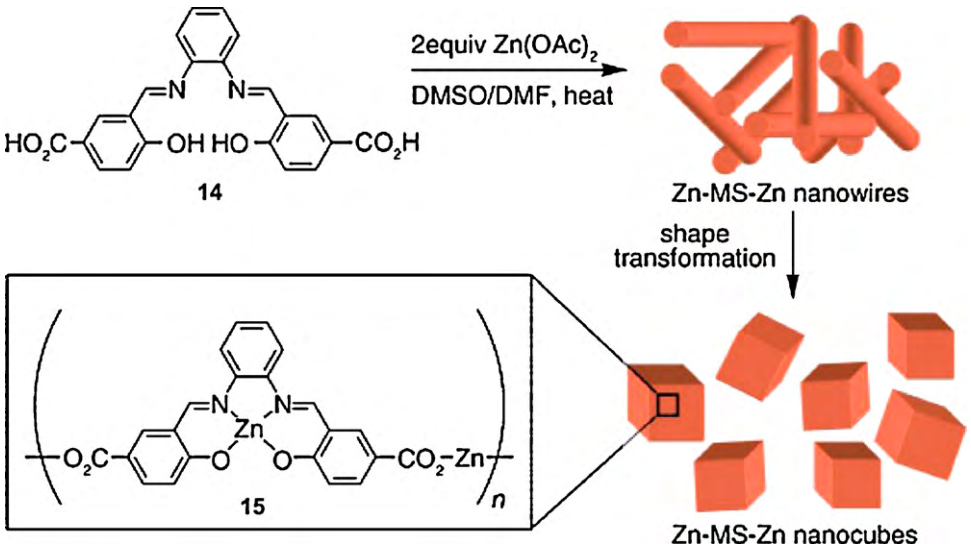

Scheme 2. Salphen **14** combines with Zn(II) to form nanowires and nanocubes, with the chemical structure depicted by **15**.

by two additional acetate groups, gave negatively charged one-dimensional chains that underwent side-by-side packing through cationic acceptor **13**. This assembly was further strengthened by the π–π interactions and hydrophobic effect perpendicular to the chain elongation, leading to the formation of the fibrous structures (Fig. 16c). Absorption and emission analysis revealed red emission when a sample of the coordination aggregate was excited at 370 nm (optimal excitation for donor **12**), which suggested effective energy transfer to the acceptor, illustrating the light-harvesting antenna effect in the nanofibers.

Oh and co-workers took advantage of the strong affinity of carboxylate groups to Zn(II) ions to create a coordination polymer that could assemble into nanofibers and further transform into nanocubes [54]. Salphen **14** (salphen = *N*,*N*′-bis(salicylidene)-*o*-phenylenediamine) was first synthesized and then combined with two equivalents of $Zn(OAc)_2$ in a 1:2 mixture of dimethylsulfoxide (DMSO) and *N*,*N*-dimethylformamide (DMF). One equivalent of Zn(II) ion was coordinated by the salphen N_2O_2 pocket resulting in a Zn(II) salphen complex, which was then linked with other complexes by the second equivalent of Zn(II) ion into a coordination polymer (**15**) (Scheme 2). The supramolecular structure of the Zn(II) salphen coordination polymer was characterized by SEM. An interesting revelation of the SEM images is that the coordination polymers organized themselves into nanowires that are ca. 40 nm in diameter and ca. 600 nm in length at an early stage of reaction (Fig. 17a and b). The nanowires then slowly aggregate together into a cubic structure and eventually transform into uniform nanocubes (Fig. 17c–h). When more nanowires were involved in the aggregation, bigger nanocubes were obtained. The formation of nanowires and nanocubes could be controlled by the reaction conditions, such as the reaction temperature, the ratio of DMSO to DMF, and the reaction time. By understanding these factors, the size and morphology of the coordination polymer aggregates with unique chemical and physical properties can be controlled.

MacLachlan and co-workers prepared a series of Zn(II)-containing salphen complexes functionalized with linear and

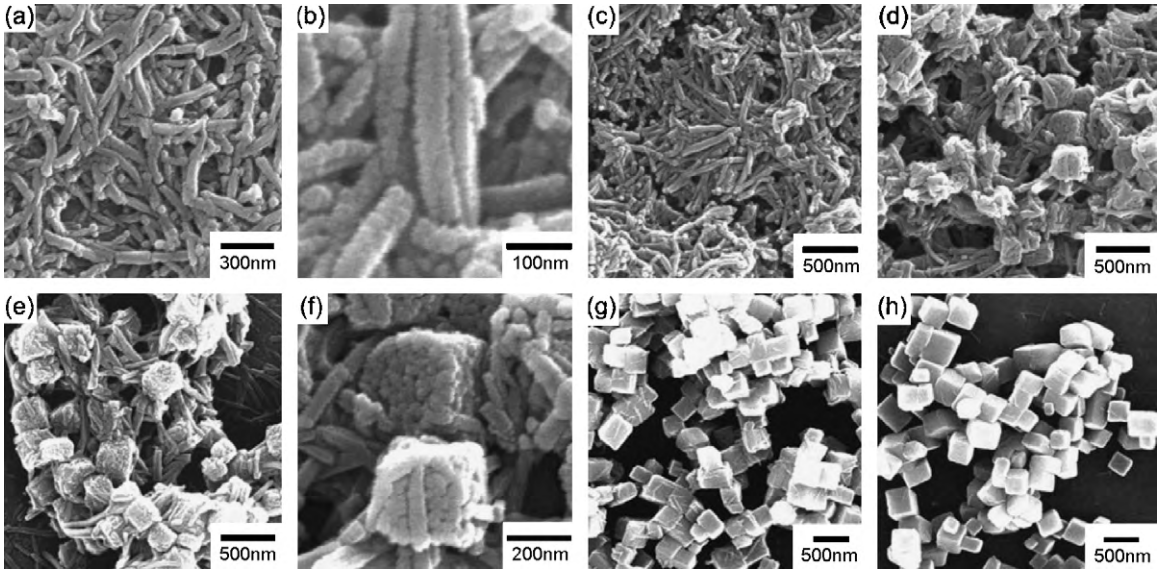

Fig. 17. (a–h) SEM images monitoring the transformation of nanowires into nanocubes.

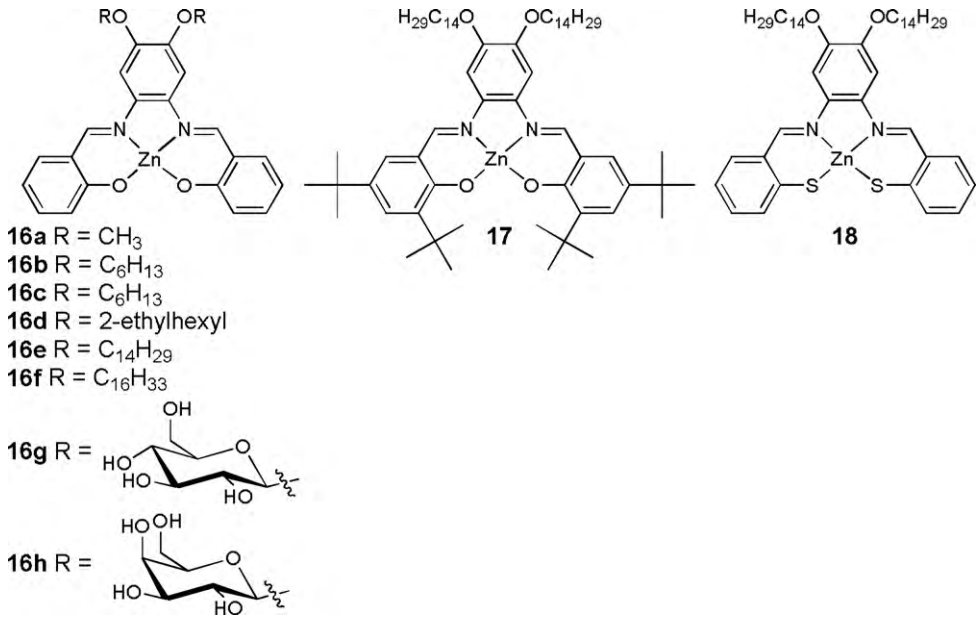

Fig. 18. Chemical structures of Zn(II) salphen complexes **16**, **17** and **18**.

branched alkoxy substituents (Fig. 18) [55]. It is noteworthy that these metal complexes were able to form luminescent gels in methanol (Fig. 19a) and aromatic solvents such as toluene, benzene and *o*-xylene, but the gels could be disrupted by the addition of pyridine (<2%). Electron microscopy of the gels prepared from methanol revealed that complexes **16** formed one-dimensional nanofibers with diameters of tens of nanometers and lengths of several microns (Fig. 19b). The aggregation was attributed to the Zn···O interactions between the Zn(II) center of a salphen unit and the neighboring phenolic oxygen. Introduction of bulky *tert*-butyl peripheral substituents on the salicylaldehyde moieties (complex **17**, Fig. 18) or replacement of the phenol groups with thiol groups (complex **18**, Fig. 18) prevented the aggregation of the Zn(II) complexes into coordination polymers and, as a result, no fiber morphology was observed under TEM. Modeling of the assembled structure illustrated that the planes of the salphen complexes were stacked in a helical conformation along the $(ZnO)_n$ polymeric backbone. This was supported by TEM in which segments of helical nanofibers could be seen as shown in Fig. 19c and d. Modification of the peripheral substituents of the Zn(II) salphen complexes with carbohydrates (glucosyl and galactosyl groups, complexes **16g** and **16h**, respectively, Fig. 18) further enhanced the helicity in the nanofibers [56]. Both TEM and AFM showed a fiber morphology similar to that of Zn(II) salphen complexes with alkoxy substituents (Fig. 19e–g). Closer observation of the fibrous superstructures by AFM revealed that the nanofibers all have left-handed helical superstructures (inset of Fig. 19g). The helical pitches measured by AFM range from ca. 30–80 nm. As the carbohydrate complexes

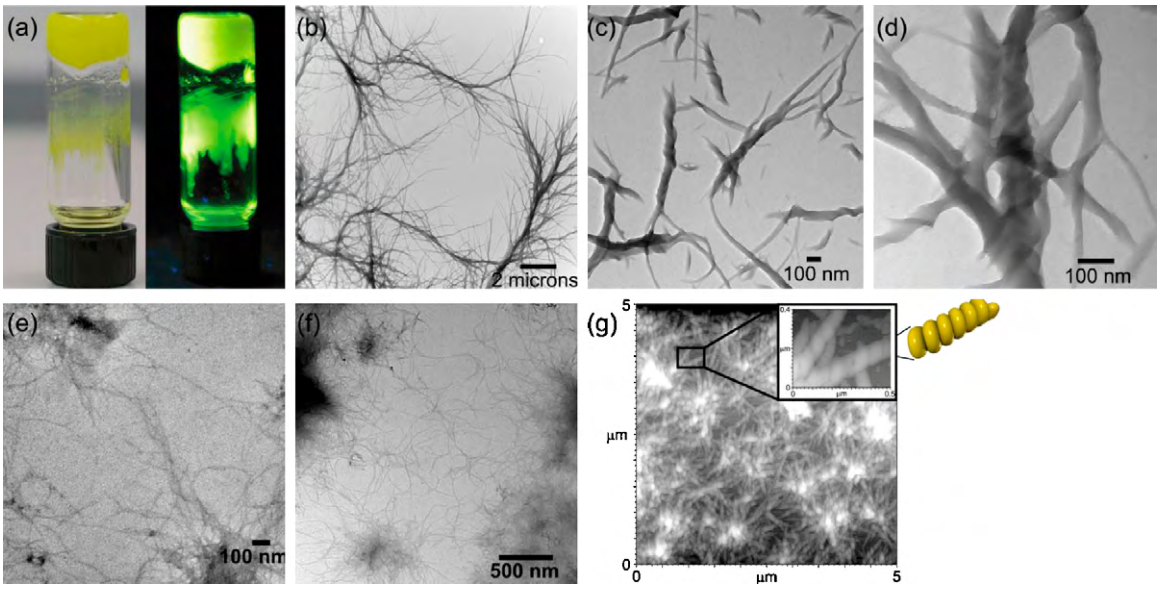

Fig. 19. (a) Photograph of luminescent gel in methanol under visible light (left) and when irradiated with UV light (right). TEM images of (b) **16e**, (c and d) segments of helical nanofibers, (e) **16g** and (f) **16h** deposited from methanol. (g) AFM image of **16g**. Inset: a closer look of the rectangular-boxed region and graphic representation of the helicity in the fibers of **16g**.
(a–d) Copyright Wiley-VCH Verlag GmbH and Co. KGaA. Reproduced with permission from ref. [55]. (e–g) Copyright Wiley-VCH Verlag GmbH and Co. KGaA. Reproduced with permission from ref. [56].

are the only source of chirality in the coordination aggregate, the substituents must be responsible for directing the helicity. It is noteworthy that the assembly in these structures is mediated by the metal; with metals other than Zn(II) (e.g., Ni(II), Cu(II)), no fibers were observed.

3.2. Static coordination polymer gels

An appealing feature of nanofibers is that they are able to trap and immobilize solvent molecules within their fibrous networks' interstitial spaces, and thus promote the formation of gels. Designing coordination polymer gelators has been of interest because the metal centers of the metallogels bestow upon them intriguing properties and applications [57]. For instance, Su and co-workers have synthesized a series of coordination polymer gels from different ratios of compound **19** (Fig. 20) and Pd(COD)$(NO_3)_2$ (COD = cycloocta-1,5-diene) in a mixed methanol/chloroform solution (Fig. 21a) [58]. In addition to the metal–ligand coordination that extends through the gel, hydrogen-bonding between the amide groups and π–π stacking between the cores of the ligand molecules help to stabilize the metallogels. SEM analysis of the xerogels of the coordination polymers revealed that the morphology of the supramolecular structures depends on the reaction ratio of the metal and **19** (Fig. 21b). Well-defined fibers with widths of ca. 30–50 nm were observed when Pd(COD)$(NO_3)_2$ and the tritopic ligand were combined in 1:1 ratio, whereas other ratios led to either spherical or porous structures (Fig. 21c and d, respectively). The metallogels formed with Pd(II) were found to have catalytic activity in the Suzuki-Miyaura coupling reaction, even at 1 mmol% of coordination polymer. Among the gels tested in the catalytic study, the fibrous metallogel (1:1 metal/**19**) showed the highest catalytic activity in the coupling reaction. Furthermore, the fibrous networked gel can be recycled several times without significant reduction in its catalytic activity. It is clear that gels formed from metallofibers have excellent potential for catalytic applications.

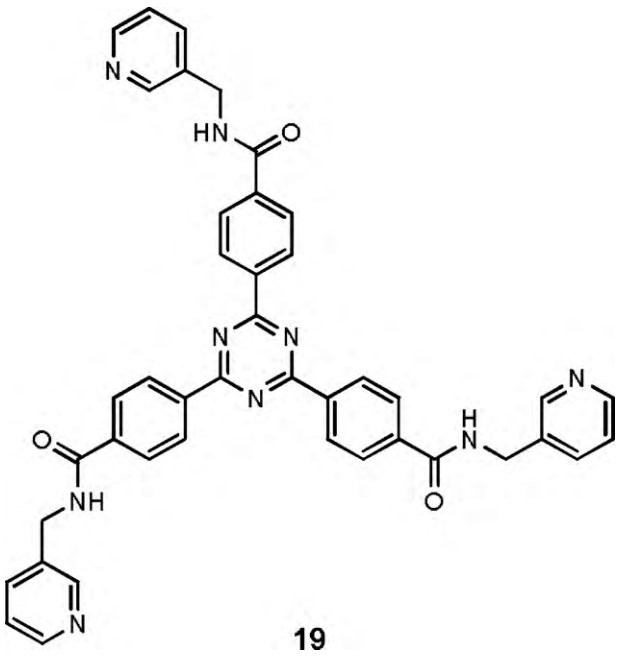

Fig. 20. Chemical structure of compound **19**.

You and co-workers applied concepts of coordination chemistry to obtain helical non-racemic polymers from achiral monomers that can form gels even without the side chain functionality (e.g., hydroxyl groups or long aliphatic chains) usually necessary to stabilize the aggregates in the gel state [59]. The coordination polymers were derived from the self-assembly of Ag(I) ions and the bent-

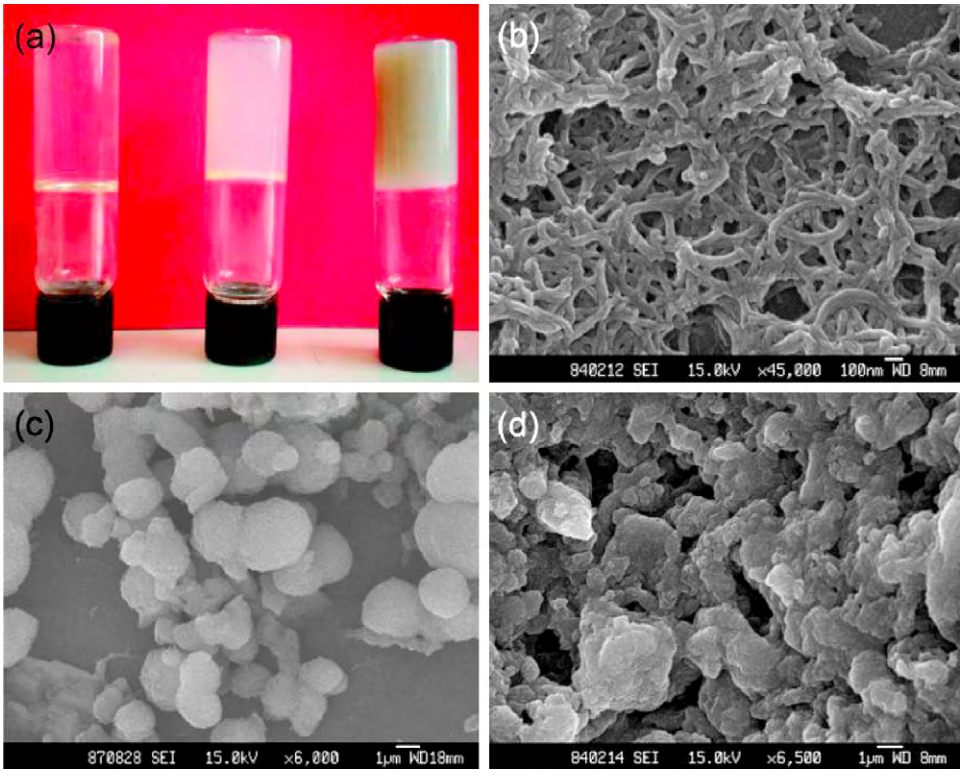

Fig. 21. (a) Photograph of metallogels with metal/**19** of 1:4 (left), 1:2 (middle) and 1:1 (right). SEM images of xerogels with (b) fibrous, (c) spherical, and (d) porous structures. Copyright 2009 American Chemical Society. Reproduced with permission from ref. [58].

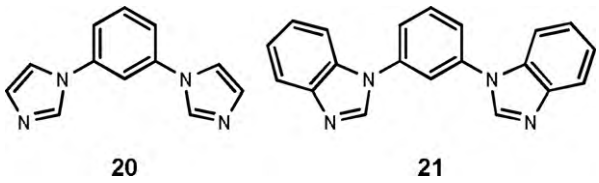

Fig. 22. Chemical structures of bisimidazole **20** and bisbenzimidazole **21**.

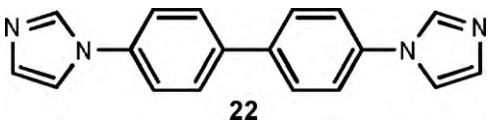

Fig. 24. Chemical structure of 4,4′-bis(1-imidazolyl)biphenyl (bibp, **22**).

shaped, achiral and ditopic imidazoles **20** and **21** (Figs. 22 and 23a). They could gelatinize solvents including DMF, glycol, and mixtures of water and organic solvents (e.g., methanol, ethanol, acetonitrile, chloroform, dichloromethane and toluene). The metallogels were found to be stable for several months at room temperature and in acidic conditions. Nonetheless, the gelation of the helical coordination polymers is dependent on the counteranion of the Ag(I) salts. For instance, $AgNO_3$ and $AgOSO_2CF_3$ generate gels, while only precipitates formed with $AgBF_4$ and $AgSbF_6$. Investigations on the assembled structure of the coordination polymer gel generated from imidazole **20** and $AgNO_3$ were performed by TEM, SEM and AFM (Fig. 23b–e). TEM images showed that the nanofibers are cylindrical aggregates with diameters of ca. 9 nm and lengths up to several microns (Fig. 23b). Closer inspection of the fibers with AFM revealed a helical structure with helical pitch of ca. 8 nm (Fig. 23d). In addition, an SEM image of the xerogel showed a well-defined fibrous network structure (Fig. 23e). The helicity of the nanofibers was further confirmed with CD. Cotton effects were observed in the CD spectra; the sign of the CD signals, however, varied with different batches of the gel prepared from the same materials. The CD data indicated that there is no control over the handedness of the helical non-racemic organization of the coordination polymers and nanofibers.

You and co-workers further expanded their investigation of coordination polymer gels in the absence of peripheral functionality, reporting the formation of a Zn(II)-containing metallogel formed upon irradiation with ultrasound [60]. The coordination polymer was prepared by reacting $Zn(OSO_2CF_3)_2$ with the simple organic bridging ligand 4,4′-bis(1-imidazolyl)biphenyl (bibp, **22**, Fig. 24). SEM of the self-assembled Zn(II) coordination polymer revealed sheet-like microparticles with uniform size and shape (Fig. 25a). Single crystals of the Zn(II) complex, obtained by slow diffusion of dioxane into a DMSO solution of the coordination polymer, were analyzed by X-ray diffraction and the structure revealed that each Zn(II) center has tetrahedral coordination geometry, bound to four imidazole nitrogen atoms from four different bibp units (Fig. 25b). The nitrogen on the other end of the coordinated bibp molecules bridges the neighboring Zn(II) centers, weaving a

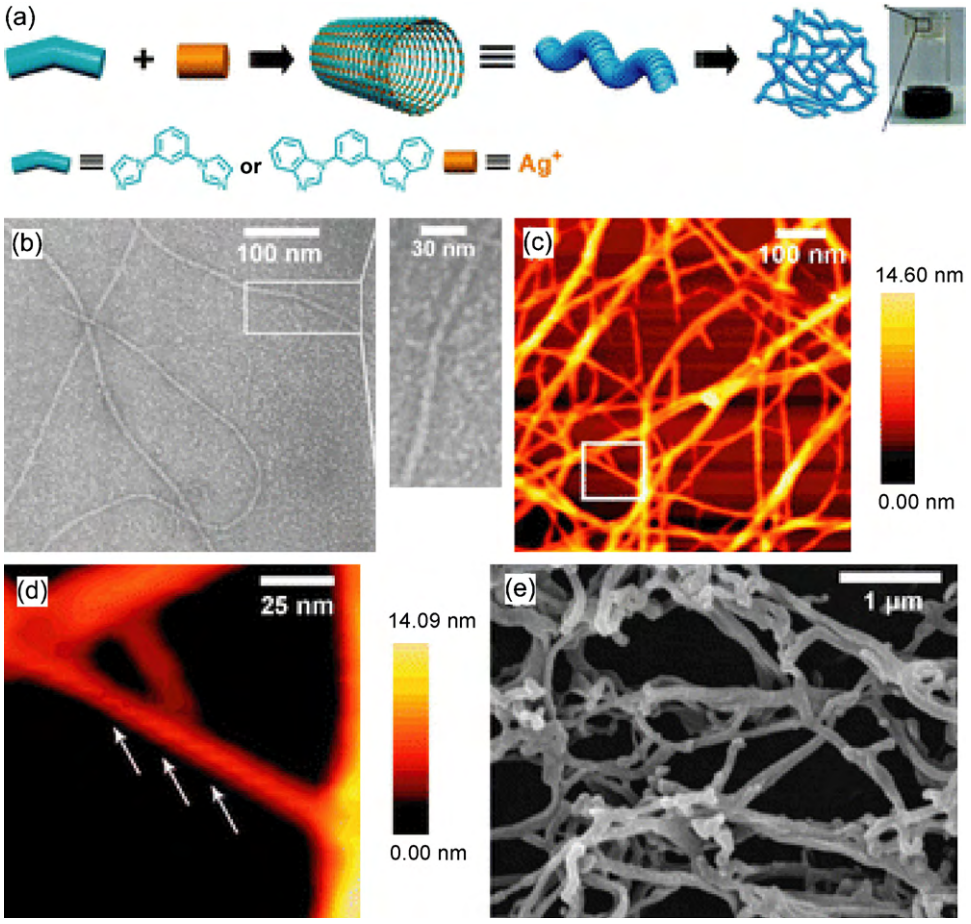

Fig. 23. (a) Schematic representation of the formation of the helical coordination polymer gelators formed from **20** and **21**. (b) TEM image of the dried gel (the sample was negatively stained with uranyl acetate solution). The inset is a magnified image of the marked area. (c) AFM (height trace, tapping mode) image of the dried gel on a mica surface. (d) A magnified AFM image of the marked area. (e) SEM image of the xerogel stained with gold.

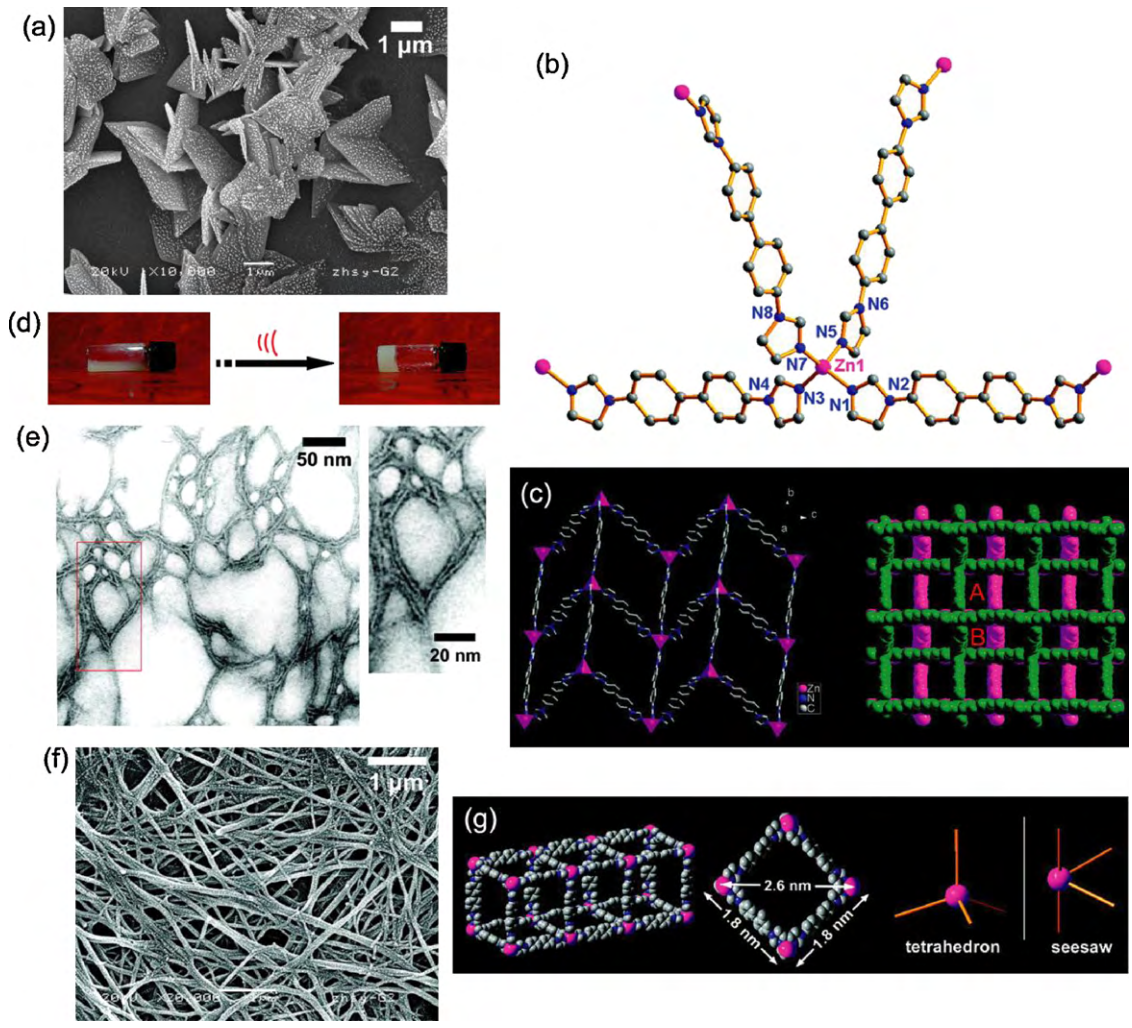

Fig. 25. (a) SEM image of the sheet-like microparticles formed from **22** before sonication. (b) Crystal structure of tetrahedral Zn(II) center with four bibp (**22**) units. (c) Two-dimensional coordination network. (d) A suspension before sonication (left) and an opaque white gel after sonication (right). (e) TEM image of the gel (negatively stained with uranyl acetate). (f) SEM image of the xerogel. (g) Metal coordination geometry is tetrahedral in the sheet-like microparticles and see-saw in the nanofibers. Copyright 2009 American Chemical Society. Reproduced with permission from ref. [60].

two-dimensional coordination network (Fig. 25c). The sheet-like microparticles of the coordination polymer did not form a gel or dissolve in methanol; however, after the suspension was sonicated for a period of 1–3 min, an opaque white gel was generated (Fig. 25d) and was found to be stable for months at room temperature. Electron microscopy was used to investigate the supramolecular structure of the gel, which should be different than the morphology before sonication (sheet-like microparticles) due to the newly discovered gelation phenomenon. High resolution TEM revealed the morphology of the metallogel to be uniform fibrous assemblies with diameters of ca. 3–4 nm and lengths up to several microns (Fig. 25e). In addition, SEM of the xerogel showed a well-structured fibrous network in which the nanofibers are 50–200 nm in diameter (Fig. 25f). The difference in diameters observed between the TEM and SEM images is ascribed to the aggregation of the nanofibers during the drying process. The morphological transformation from sheet-like microparticles to nanofibers originated from the change in coordination environment of the Zn(II) centers before and after irradiation with ultrasound. Solid-state ^{13}C NMR spectroscopic experiments on the microparticles and xerogel provided information about the geometrical change at the metal centers from the difference in chemical shifts of the aromatic carbon peaks in both samples. The sonication presumably facilitated the breaking and reorganizing of the coordination bonds and changed the geometry of the Zn(II) centers from tetrahedral in the sheet-like microparticles to see-saw geometry in the nanofibers (Fig. 25g) that results in a fibrous network, giving a gel.

Vittal and co-workers reported a hydrogel generated from $Mg(CH_3COO)_2{\cdot}4H_2O$ and the basic aqueous solution of *N*-(7-hydroxyl-4-methyl-8-coumarinyl)-alanine (**23**, Fig. 26) [61]. The carboxylate oxygen atoms of **23** coordinated to the neighboring

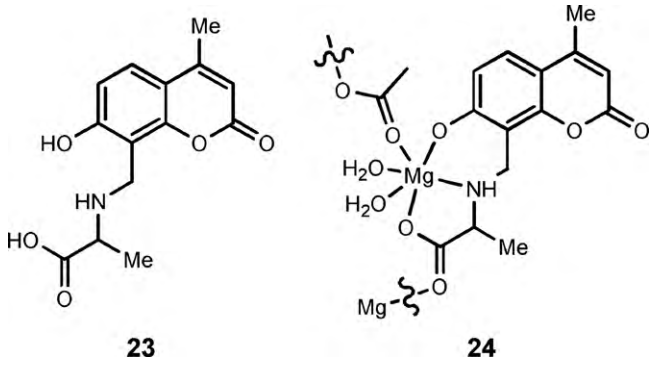

Fig. 26. Chemical structure of the free ligand **23** and schematic representation of the proposed coordination polymer **24**.

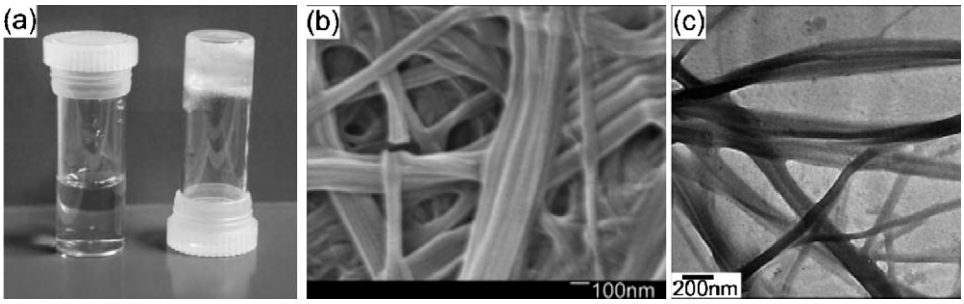

Fig. 27. (a) Photograph of ligand **23** in water (left) and hydrogel (right). (b) SEM and (c) TEM images of the xerogel of coordination polymer **24**. Copyright Wiley-VCH Verlag GmbH and Co. KGaA. Reproduced with permission from ref. [61].

metal center to form the coordination polymer **24**, shown in Fig. 26. The coordination polymer gel is thixotropic and sensitive to pH. The gel liquefied upon shaking and reformed into a gel upon standing (Fig. 27a). In addition, it turned into a clear solution at pH 2 because protonation of the ligand disrupted the structure, but this was reversible and a gel was formed when the pH was adjusted to 8. The morphology of the hydrogel was analyzed by electron microscopy. From the SEM and TEM micrographs of the xerogel, polymer **24** self-assembled into bundles of nanofibers and further organized into a well-defined network capable of trapping solvent molecules (Fig. 27b and c). The fibers are several microns long and the diameters are 50–150 nm. Photophysical studies of the hydrogel showed that it exhibited strong blue emission with peak maximum at $\lambda = 455$ nm when excited at $\lambda = 360$ nm. The intensity of the fluorescence was enhanced significantly in the gel form compared to free ligand **23** and a solution of coordination polymer **24**. Vittal and co-workers further reported a coordination polymer gel produced from linear bridging ligands and Ni(II) ion in an acidic medium [62]. An initial morphological study of the gel with SEM revealed no fibrous structure. The gel was then diluted to half the original concentration and homogenized by stirring. After that, it was subjected to electrospinning to generate bundles of nanofibers, and the fiber morphology was confirmed by SEM, TEM and AFM. The electrospun fibrous bundles are ca. 100 nm in diameter and centimeters in length, with individual fibers having a diameter of ca. 10 nm. It is noteworthy that the electrospun fibers exhibited strong photoemission in the visible and UV regions, and field emission with low turn-on fields for metal-coordinated nanofibers [63].

3.3. Dynamic coordination polymer gels

One-dimensional assemblies of coordination complexes are attractive for their electronic, magnetic and optical properties [64]. However, solubility of the supramolecular assemblies has always been a challenge, and has limited the ways in which coordination polymers can be manipulated. Kimizuka and his co-workers have focused on this area of research and reported a series of coordination polymers with solubility promoted by incorporating lipophilic triazole bridging ligands into the polymeric main chains, or by introducing lipid-like counteranions in the vicinity of the metal centers. Lipophilic Co(II) complexes **25** and **26**, shown in Fig. 28, were synthesized with ligands 4-hexadecyl-1,2,4-triazole (**27**) and 4-dodecyloxypropyl-1,2,4-triazole (**28**) [65]. The long chains on these ligands are used to enhance the solubility of the complexes and the polymeric aggregates. When complexes **25** and **26** were dissolved in chloroform, blue gels were obtained at low concentrations (10 and 0.007 wt% for **25** and **26**, respectively) as depicted in Fig. 29a. The blue color, characteristic of Co(II) in a tetrahedral (T_d) coordination environment, revealed the geometry at the metal center. The gels were studied by AFM, SEM and TEM (Fig. 29c–f) to gain insight into the supramolecular organization. Complex **25** showed crystalline nano-aggregates with lengths of ca. 500–1500 nm and widths of 30–50 nm (Fig. 29e) by TEM. On the other hand, the AFM and TEM micrographs of complex **26** revealed fibrous networks in which the nanofibers are 5–30 nm in diameter. In addition, the xerogel of complex **26** displayed thicker fibers (ca. 100 nm in diameter) by SEM due to the aggregation of the nanofibers during the drying process. That complex **25** did not develop into a fibrous network is related to its lower gelation ability compared to complex **26**. It is interesting to note that no fiber morphology was observed with either of the lipophilic ligands alone. Therefore, the fibrous nanostructure is attributed to the self-assembly of the cobalt(II) complexes in chloroform, and the cobalt centers adopted a T_d geometry along the main chain (Fig. 29g). A special feature of these gels is that they turn into pale pink solutions upon cooling (Fig. 29b) and return to blue-colored gels upon heating. This heat-induced gelation is contrary to the behavior of conventional gels (i.e., gelation upon cooling and dissolution upon heating). The sol-to-gel transition is reversible with subsequent cooling and heating cycles. The pink color indicates that the cobalt(II) centers are in octahedral (O_h) coordination environment (Fig. 29h) and the reversible geometric transformation at cobalt was confirmed by UV–visible spectroscopy. The authors proposed that the coordination polymer with O_h metal centers in the solution state has a rod-like structure with the lipophilic chains aligned perpendicular to the main chain. However, no superstructures were observed by TEM.

The gel transition is also toggled by the addition of long-chained alcohols including 1-dodecanol and 1,12-dodecanediol [66]. When either alcohol was added to a pink solution of complex **26** obtained at 0 °C, the solution turned blue within ca. 5 min and a gel formed within ca. 10 min. Again, the color change corresponded with a change in the geometry of the complex from O_h to T_d, which

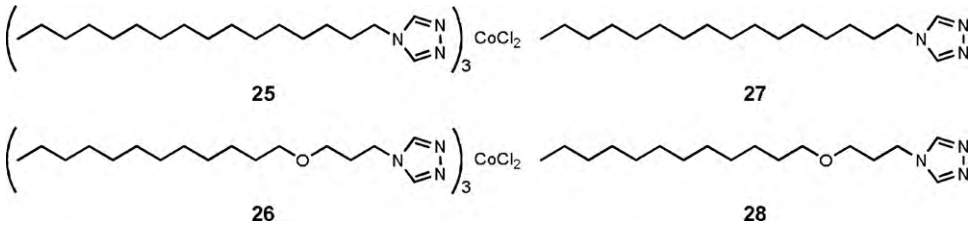

Fig. 28. Chemical structures of lipophilic Co(II) complexes **25** and **26**, and ligands **27** and **28**.

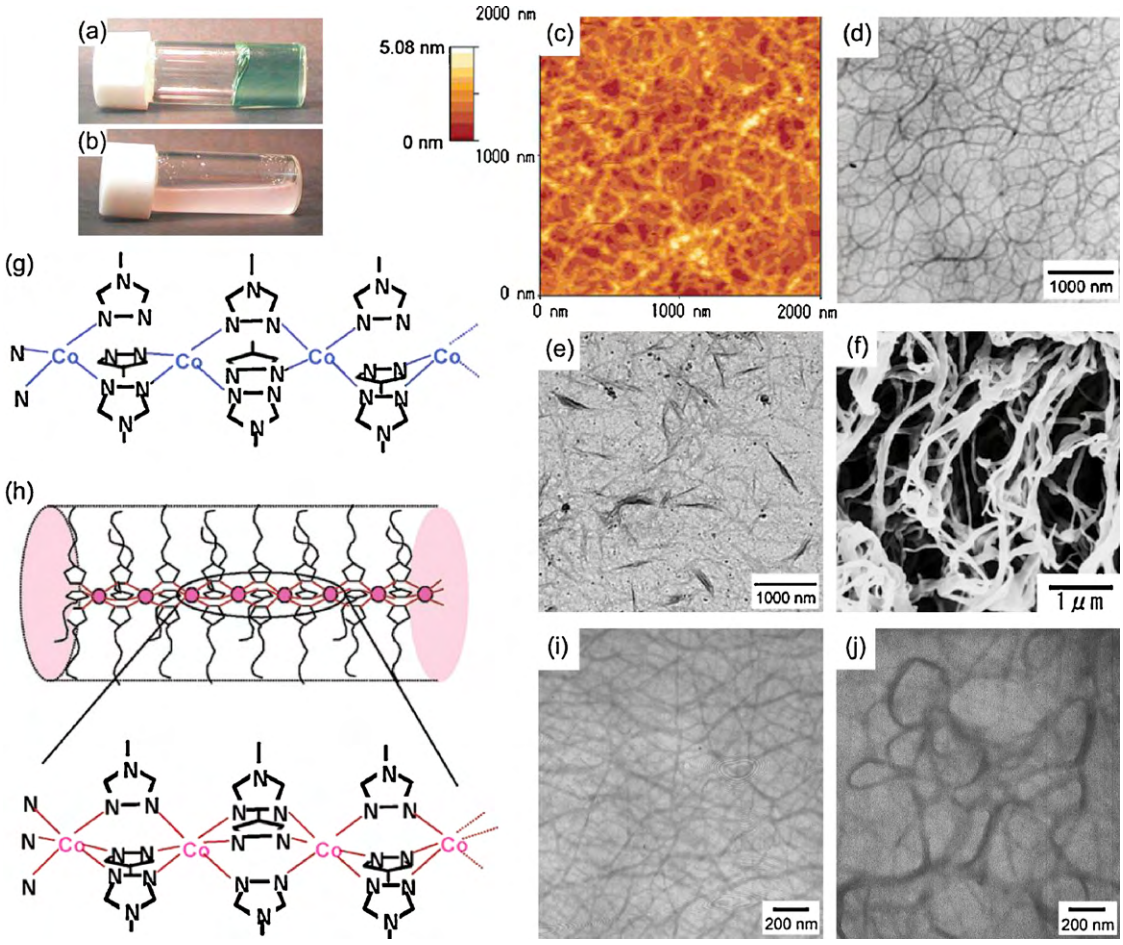

Fig. 29. Photographs of complex **26** in chloroform at (a) 25 °C (blue gel) and (b) 0 °C (pale pink solution). (c) AFM and (d) TEM images of complex **26**. (e) TEM image of complex **25**. (f) SEM image of the xerogel of complex **26**. Schematic representations of (g) polymeric T_d complex and (h) polymeric O_h complex.
Reproduced with permission from ref. [65]. Copyright 2004 American Chemical Society. TEM images of complex **26** with (i) 1-dodecanol and (j) 1,12-dodecanediol. Reproduced with permission from ref. [66]. Copyright 2008 The Chemical Society of Japan.

was confirmed by UV–visible spectroscopy. TEM analysis of the gels showed networks of fibrous structures with widths of ca. 100 and 500 nm for the samples prepared with 1-dodecanol (Fig. 29i) and 1,12-dodecanediol (Fig. 29j), respectively. Binding of the long-chained alcohols to the surface of the coordination polymer through hydrogen-bonding to the anions (ROH···Cl^-) induces the transformation of the geometry to T_d in order to fit the guest molecules, the long chains of ligand **28** and alcohol molecules aligning perpendicular to the polymer chain. These studies indicate that the coordination geometry at cobalt centers can be modified by changing the temperature and by binding guests, triggering a change of color and morphology.

Lipophilic, linear polymeric Fe(II) triazole complex **29** containing octahedral metal centers was prepared with ligand **28** (Fig. 30) [67]. Polymer **29** (Fig. 31a and b) exhibits spin-crossover behavior between low spin (LS) and high spin (HS), and each spin state of the Fe(II) triazole complexes has a characteristic color (purple = LS and yellow or colorless = HS). The spin-crossover characteristics are usually affected by the type of substituent on the bridging ligands and the counteranions incorporated. Complex **29**, a purple solid, gave a pale yellow gel at room temperature in chloroform (Fig. 31c). The color indicated that Fe(II) centers changed from LS state to HS state after gelation. This is attributed to the elongation of the Fe—N coordination bonds in solution, weakening the ligand field strength and thus favoring the HS state. The supramolecular structure of the gel was investigated by TEM and nanofiber superstructures with widths of 3–5 nm could be observed (Fig. 31c). Similarly, the coordination gel obtained with complex **26** turned into a yellow solution upon cooling to 5 °C. When the yellow chloroform solution of complex **29** was cast onto a solid substrate and dried into a transparent film, the color changed to purple upon solvent evaporation due to spin crossover to the LS state (Fig. 31d). As the purple-colored film was heated, it returned to a yellow color at 80 °C (Fig. 31e). This reversible, temperature-dependent spin crossover was monitored by UV–visible spectroscopy. In addition, the temperature of the spin crossover for complex **29** is affected by the presence of long-chained alcohols such as 1-dodecanol and 1-tetradecanol, which are able to hydrogen-bond to the chloride counteranions of the iron complex (Fig. 31f). When chloroform solutions of complex **29** combined with equimolar alcohol were cast as films, UV–visible spectroscopic studies showed that the LS-to-HS transition temperatures were lowered (55 and 68 °C for 1-dodecanol and 1-tetradecanol doping, respectively) compared to that before alcohol doping (80 °C), thus indicating that the LS state was destabilized by the binding of guest alcohol molecules.

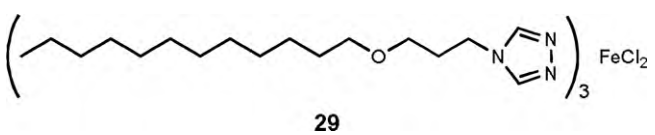

29

Fig. 30. Chemical structure of lipophilic Fe(II) complex **29**.

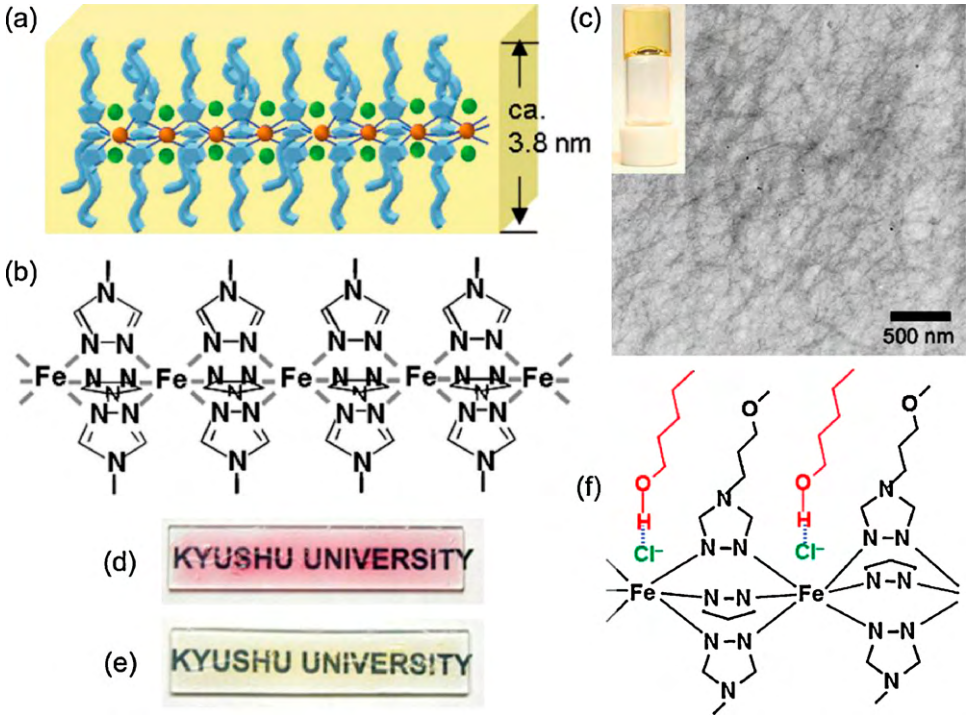

Fig. 31. Schematic representations of (a and b) the lipophilic polymeric Fe(II) complex **29**. (c) The yellow gel (20 °C in chloroform) and TEM image of complex **29**. Photographs of cast films at (d) 20 and (e) 80 °C. (f) Schematic representation of the long-chained alcohols hydrogen-bonded to the chloride counteranions. Copyright 2006; Reproduced with permission of John Wiley & Sons, Inc from ref. [67].

Iron(II) triazole complexes **30** and **31** were developed with ligand **28** and chromophoric counteranions 9,10-dimethoxyanthracene-2-sulfonate (Anth-SO_3^-) and 1-pyrenesulfonate (Py-SO_3^-) (Fig. 32) [68], and their fluorescence properties were studied. The anionic chromophores are located in the vicinity of iron centers along the coordination polymeric main chain. Toluene solutions of complexes **30** and **31** prepared at different temperatures, where they exhibited different spin states, were dried and then the solids analyzed by AFM. Fibrous nanostructures with widths of 20–30 nm and heights of ca. 1.5 nm were observed for complexes **30** and **31** in the LS state (10 and 4 °C, respectively) (Fig. 33a and c), but only irregular structures or dot-like aggregates could be seen in the HS state (40 and 45 °C, respectively) (Fig. 33b and d). This change in the morphology of the self-assembled structures from LS to HS (nanofibers to dot-like structure) upon heating gradually diminished the fluorescence intensities of the counteranions. Therefore, the fluorescence of the chromophores was related to the spin state of the metal center and the morphology of the coordination aggregate.

The morphology of the coordination polymer can be regulated by solvent and external stimuli such as temperature and irradiation. For instance, the bridging ligand was modified by incorporating an azobenzene chromophore, which can undergo photoisomerization upon irradiation, within the lipophilic substituent of triazole (**32**, Fig. 34). The new linear Fe(II) triazole complex (**33**) formed from this ligand has iron centers in O_h coordination environments (Fig. 35a) [69]. A structural study was performed on complex **33** prepared in chloroform and a fibrous morphology was observed by AFM (Fig. 35b). The nanofibers were ca. 6.9 nm in diameter and 10–100 nm in length. No gelation occurred for complex **33** in chloroform, but when chlorocyclohexane was used as the solvent, a yellow-colored coordination polymer gel formed in 6–24 h (Fig. 35c). AFM of the sample prepared in chlorocyclohexane showed oriented arrays of aggregates with lengths over 400 nm and heights of ca. 1 nm (Fig. 35h). The morphology is different than that observed from the chloroform sample. Moreover, the average distance between the linear structures in Fig. 35h is ca. 6 nm, which is smaller by 1 nm compared to the nanofibers in Fig. 35b. SEM of the xerogel of complex **33** showed ultra-thin nanosheets with a thickness of ca. 10 nm (Fig. 35g). The formation of the nanosheets was derived from the two-dimensional alignment of the linear aggregates, which can be rationalized by the height measured by AFM, in agreement with the thickness of the nanosheets observed by SEM. The *trans*-to-*cis* photoisomerization of the azobenzene units was studied by irradiating gels of complex **33** with UV light at 365 nm. Upon irradiation, the yellow gel liquefied into an orange solution (Fig. 35d). The coordination sphere of the metal in complex **33** remained unchanged after isomerization of the azobenzene, but the gel was liquefied as the bent-shaped cis-azobenzene disrupted the packing of the lipophilic substituents (Fig. 35a). AFM of the UV-irradiated sample revealed a fiber morphology (Fig. 35i) similar to that in Fig. 35b (chloroform sample). An interesting feature of the orange solution is that upon irradiating with visible light, *cis*-to-*trans* photoisomerization of the azobenzene units took place and

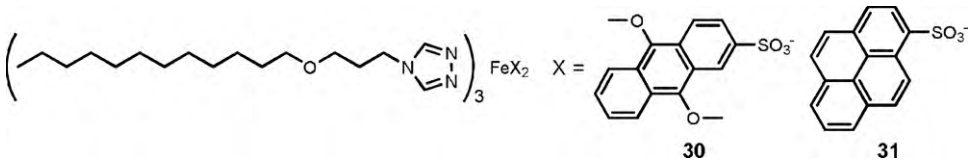

Fig. 32. Chemical structures of lipophilic Fe(II) complexes **30** and **31**.

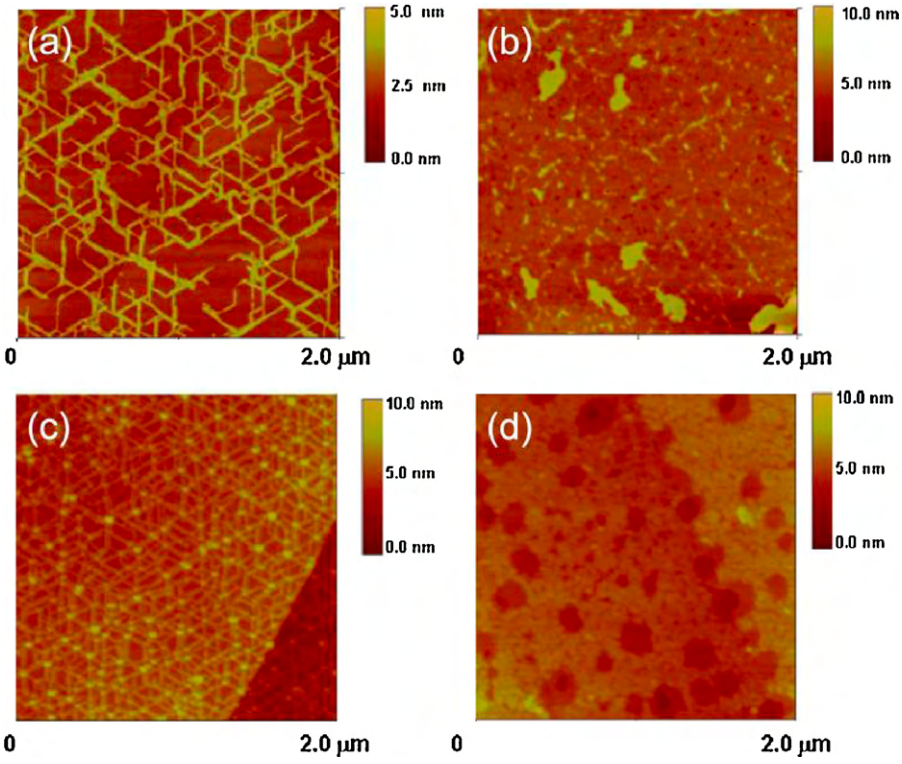

Fig. 33. AFM images of complex **30** in the (a) LS and (b) HS states, and complex **31** in the (c) LS and (d) HS states. Copyright 2008 The Chemical Society of Japan. Reproduced with permission from ref. [68].

the color of the solution returned to yellow and a yellow-colored gel formed after sitting in the dark for 20 min. The gel-to-sol transition induced by UV and visible light, triggered by the *cis–trans* isomerization, is reversible and the cycle could be repeated multiple times.

The iron centers in most Fe(II) triazole complexes tend to exhibit the LS state in the solid or gel form, and HS state in solution. This is closely related to the bonding distance between iron and the bridging ligand, which is lengthened in solution and results in the destabilization of the LS state. Iron(II) triazole complexes **34** and **35** with lipophilic counteranions were synthesized and both have a purple color at room temperature when they are dissolved in toluene, indicating that the complexes remain in the LS configuration in solution (Fig. 36) [70]. As the temperature of the solution was raised, spin crossover occurred; this LS–HS transition is reversible with subsequent cooling and heating cycles (Fig. 37a). The unusual LS state in toluene was ascribed to the solvophobic Fe(II) triazole complexes minimizing contact with the non-polar solvent molecules by shrinking the Fe—N bonds, thereby strengthening the ligand field and leading to the stabilization of the LS state. AFM images of complexes **34** and **35** were obtained to investigate the superstructures of the complexes in different spin states (Fig. 37b–e). Nanofibers with widths of 20–30 nm and heights of ca. 7 nm were observed for the LS state (Fig. 37b and d) while the HS state gave only fragmented structures or dots (Fig. 37c and e). Since the coordination number at the metal centers should not change during spin crossover, the change in spin state with respect to temperature apparently involves the fragmentation of the fibrous nanostructures (breaking of the coordination bonds). Thus, the transition between LS and HS is regulated by supramolecular self-assembly of the iron complex.

Kimizuka and co-workers have also prepared a family of one-dimensional halogen-bridged, mixed valence Pt complexes from $[Pt(en)_2][PtCl_2(en)_2](ClO_4)_4$ with lipid counteranions (**36**–**43**, Fig. 38) [71]. These linear complexes $[Pt(en)_2][PtCl_2(en)_2]$(**36**–**43**)$_4$ are composed of $[Pt(II)(en)_2]$ and $[Pt(IV)Cl_2(en)_2]$ that are bridged by chloride, and the charge of each of the platinum centers is balanced by two lipid anions (Fig. 39). $[Pt(en)_2][PtCl_2(en)_2]$(**36**–**43**)$_4$ have intense colors that originate from the intervalence charge transfer (CT) absorption of the chloro-bridged Pt(II)/Pt(IV) along the coordination polymer backbones. Different colors could be obtained by changing the CT absorption. There are three factors that affect the CT absorption of the mixed valence Pt complexes: the nature of the counteranions, the solvent, and the

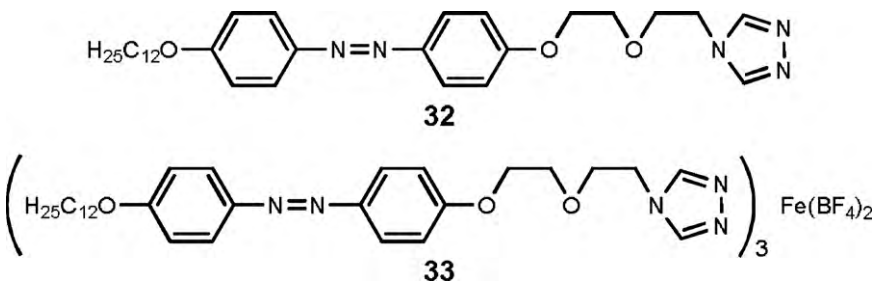

Fig. 34. Chemical structures of ligand **32** and lipophilic Fe(II) complex **33**.

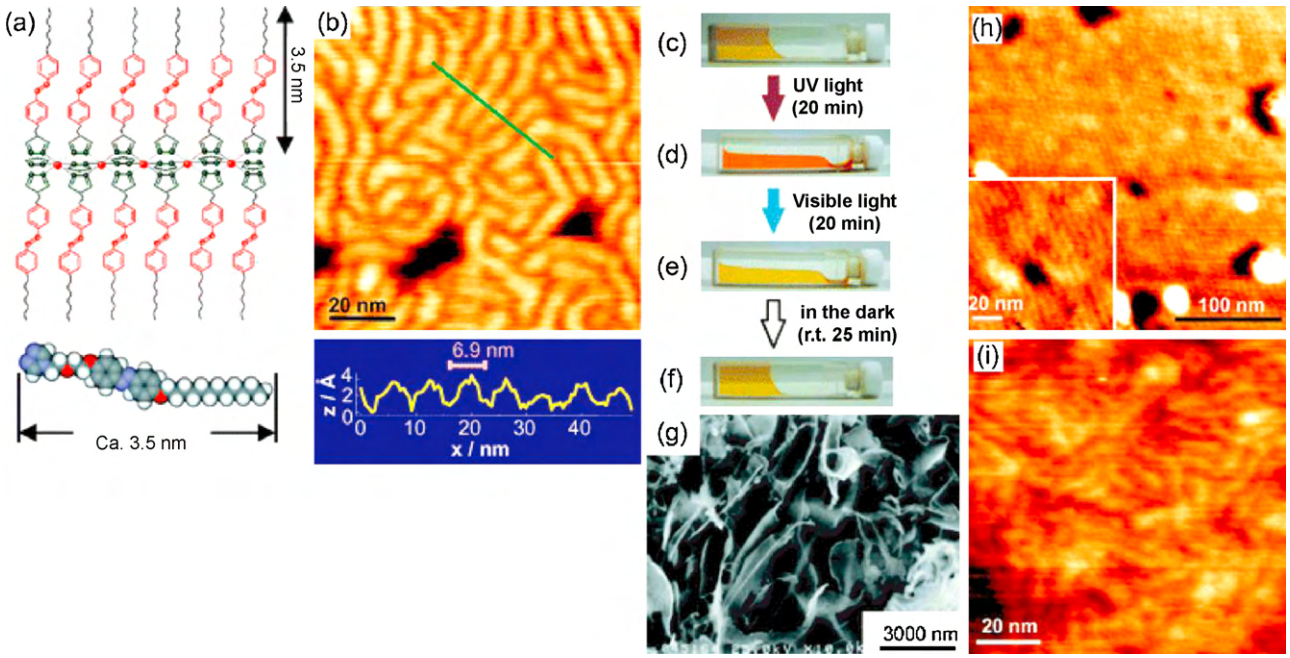

Fig. 35. (a) Schematic representation of lipophilic polymeric Fe(II) complex **33**. (b) AFM of the sample prepared in chloroform. (c–f) Photographs of complex **33** in chlorocyclohexane at room temperature: (c) before irradiation, (d) after irradiation with UV light (365 nm), (e) after irradiation with visible light (546 nm), and (f) after storage in the dark for 25 min. (g) SEM of the xerogel. (h) AFM of the sample prepared in chlorocyclohexane (h) before and (i) 2 min after irradiation with UV light (365 nm). Copyright 2006 The Royal Society of Chemistry. Reproduced with permission from ref. [69].

temperature. As already noted, those three factors can also influence the supramolecular self-assembled structures of coordination polymers. The incorporated counteranions promoted solubility in organic solvents, but their sizes affect the distance between the Pt(II) and Pt(IV) centers and, as a result, induced a change in the CT absorption. In general, bulkier counteranions (e.g., **39**, **40**) increase the intrachain Pt(II)–Pt(IV) distance and red-shift the CT absorption with respect to the reference complex $[Pt(en)_2][PtCl_2(en)_2](ClO_4)_4$, while smaller anions decrease the distance and show a blue-shifted band (e.g., with **41**) [71a]. In addition, the complexes are strongly solvatochromic. For example, $[Pt(en)_2][PtCl_2(en)_2](\mathbf{43})_4$, an orange solid, gave a red solution when dissolved in dichloromethane, while an orange solution was obtained in chloroform [71c].

The lipid counteranions and solvents not only influence the color of the Pt complexes, but also the morphology of the superstructures of the coordination polymers. Complexes of $[Pt(en)_2][PtCl_2(en)_2](\mathbf{36}–\mathbf{43})_4$ exhibited different morphologies when imaged by TEM (Fig. 40a–g). Since all of the complexes contain the same chloro-bridged Pt(II)/Pt(IV) backbone, the morphology difference must be derived from the counteranions and solvents. Nanofibers with widths of 20–100 nm and lengths of over 20 microns were observed for $[Pt(en)_2][PtCl_2(en)_2](\mathbf{43})_4$ in chloroform (Fig. 40f), but only nanorods, nanocrystals or tape-like structures were obtained with other counteranions or samples prepared in different solvents (Fig. 40a–e and g). Another phenomenon of the linear mixed valence complexes is that the intense color tends to fade out and eventually disappear as the temperature of the solution increases. The absence of color is a sign that the complexes $[Pt(en)_2][PtCl_2(en)_2](\mathbf{36}–\mathbf{43})_4$ have dissociated into $[Pt(en)_2](\mathbf{36}–\mathbf{43})_2$ and $[PtCl_2(en)_2](\mathbf{36}–\mathbf{43})_2$ at elevated temperatures, eradicating the CT band. Different solvents and counteranions rendered different thermal stability to the linear Pt complexes, and the dissociation of the coordination polymers at elevated temperatures resulted in different morphologies observed by TEM. For example, $[Pt(en)_2][PtCl_2(en)_2](\mathbf{40})_4$ gave a tape-like morphology before heating (Fig. 40b), but crystalline aggregates with widths of 50–200 nm and lengths of 400–550 nm were observed upon heating to 60 °C (Fig. 40h). After the sample cooled back to room temperature, fibrous nanostructures with a minimum width of 18 nm and lengths of 700–1700 nm were obtained (Fig. 40i). The formation of the nanofibers is ascribed to the self-assembly of the dissociated components in solution (Fig. 40j) [71d]. It is noteworthy that as the samples cooled, the intense color from the CT band returned. However, for $[Pt(en)_2][PtCl_2(en)_2](\mathbf{36})_4$, only globular aggregates with diameters of 100–300 nm were observed after cooling the sample from 60 to 25 °C (Fig. 40j) [71a]. The lin-

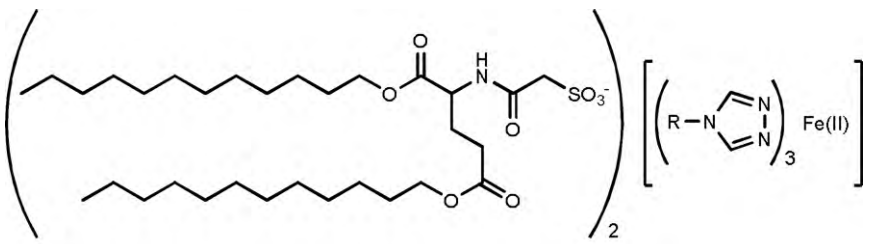

34 R = NH_2
35 R = C_2H_4OH

Fig. 36. Chemical structures of lipophilic Fe(II) complexes **34** and **35**.

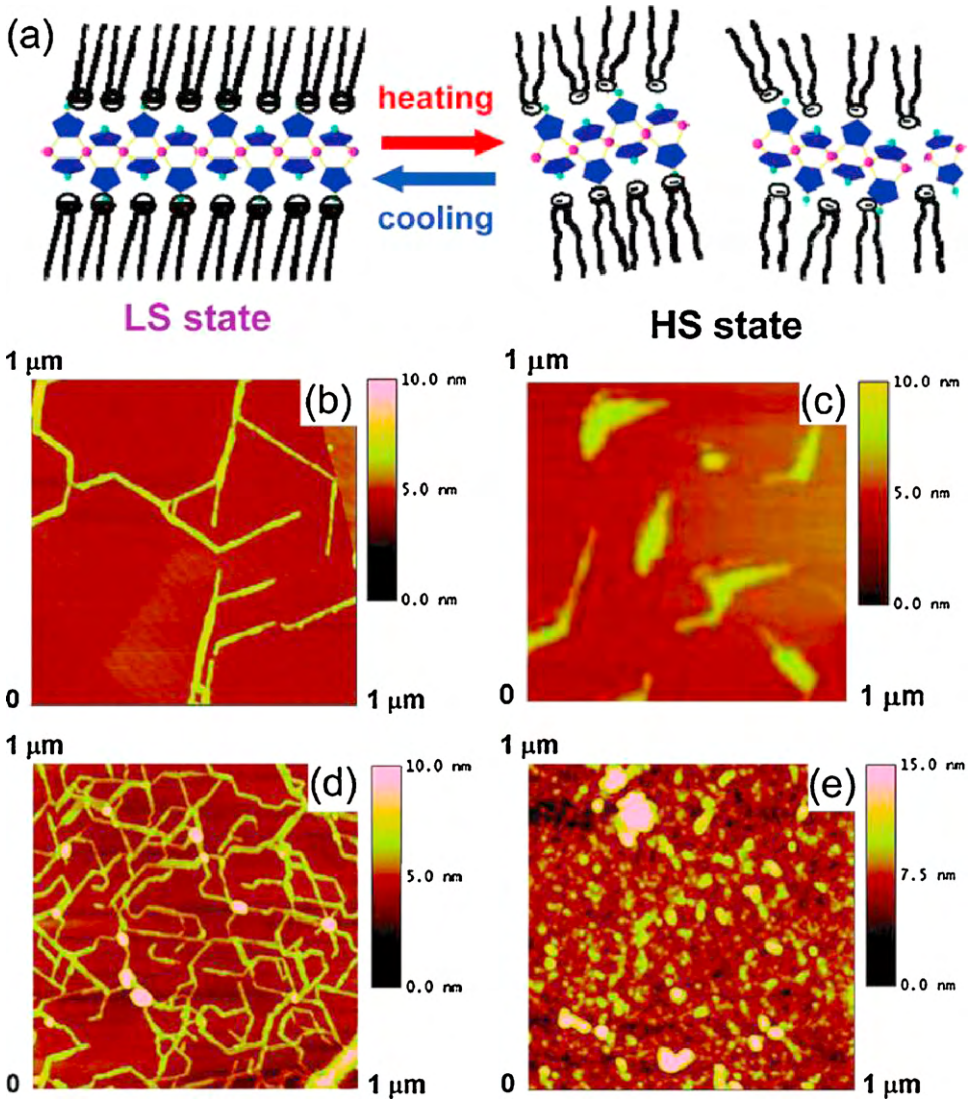

Fig. 37. (a) Schematic representation of the reversible LS-HS transition with cooling and heating cycles. AFM images of complex **34** in the (b) LS and (c) HS states, and complex **35** in the (d) LS and (e) HS states.

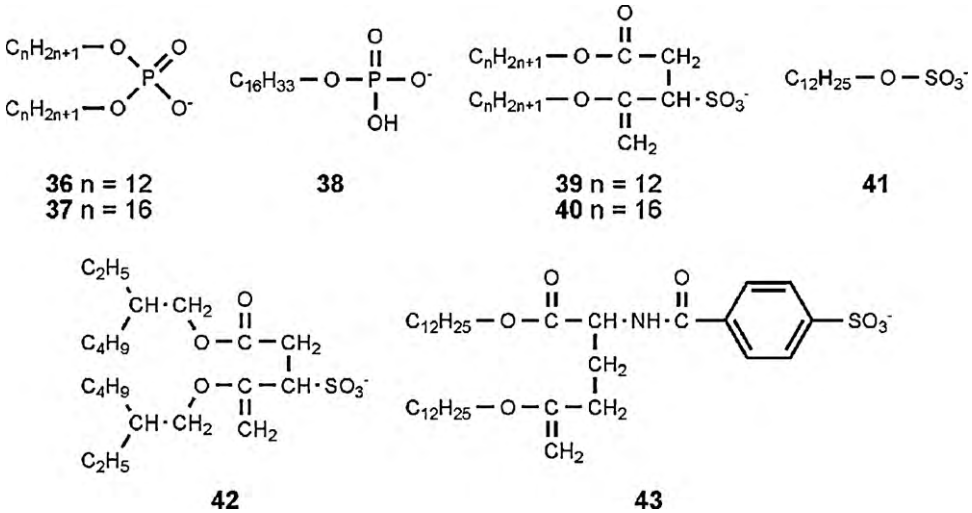

Fig. 38. Chemical structures of lipid counteranions **36**–**43**.

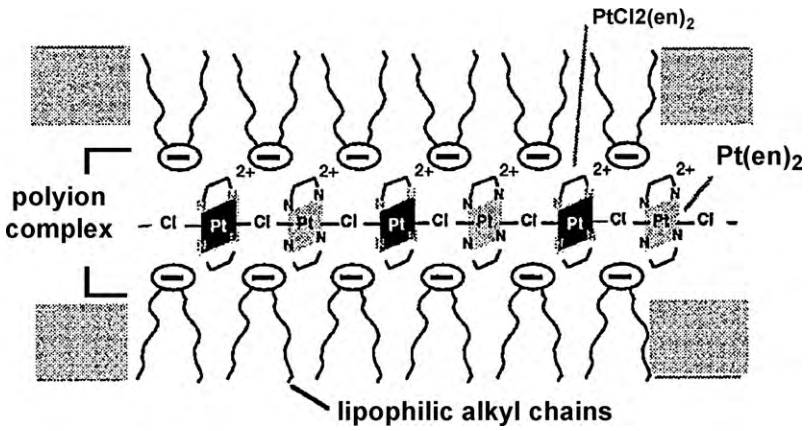

Fig. 39. Schematic representation of polymeric Pt complexes with lipid counteranions.
Copyright 1998 The Chemical Society of Japan. Reproduced with permission from ref. [71b].

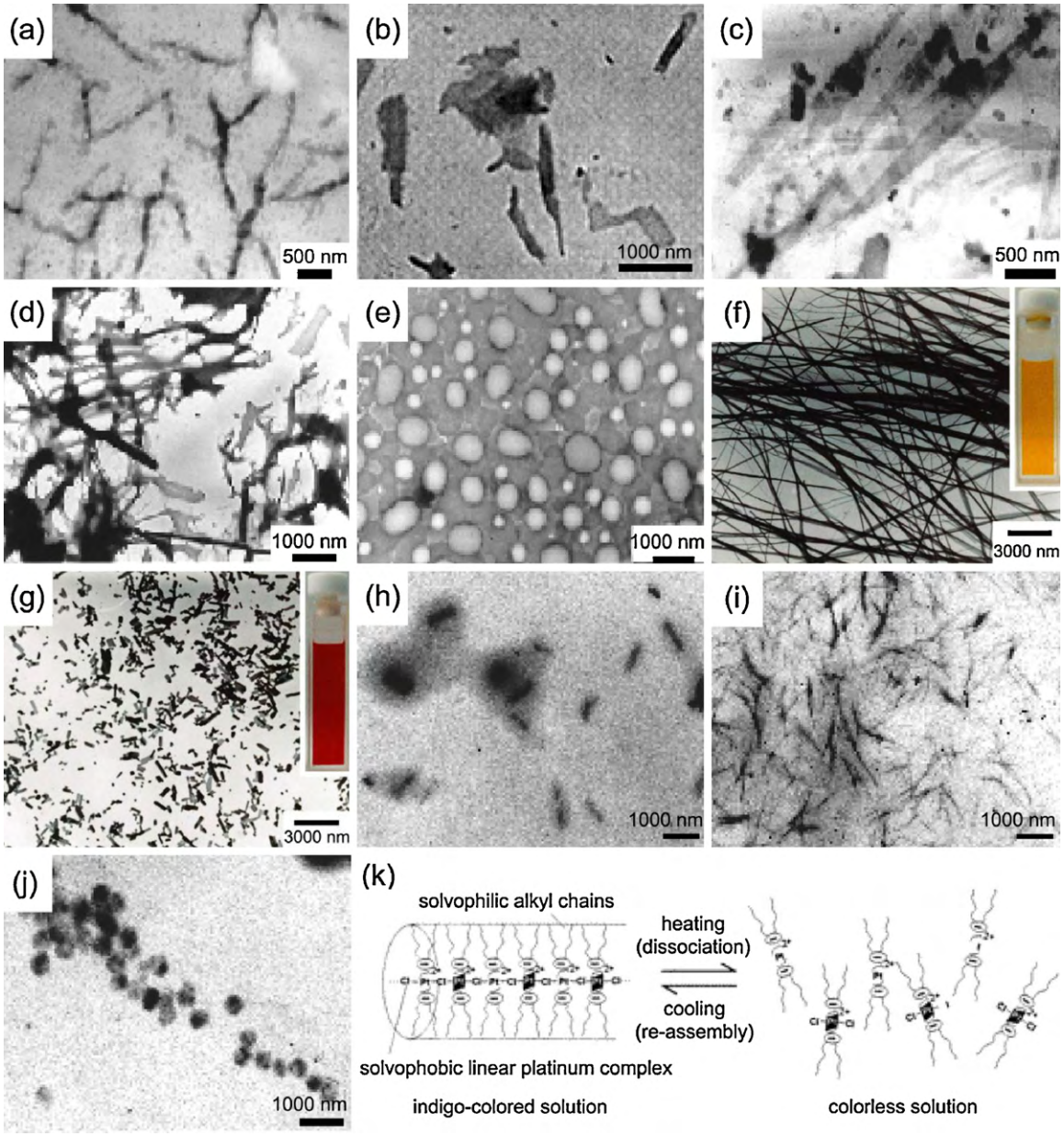

Fig. 40. TEM images of the mixed valence Pt complexes with lipid counteranions (a) **36**, (b) **39**, (c) **40**, (d) **41**, (e) **42**, (f) **43** in chloroform, (g) **43** in dichloromethane, (h) **40** at 60 °C, (i) **40** after cooling from 60 °C to room temperature, and (j) **36** after cooling from 60 °C to room temperature, respectively. (k) Schematic representation of the reversible dissociation/re-assembly process.
(a, c–e, h–k) Reproduced with permission from ref. [71a]. Copyright 2000 American Chemical Society. (b) Reproduced with permission from ref. [71b]. Copyright 1998 The Chemical Society of Japan. (f and g) Reproduced with permission from ref. [71c]. Copyright 2002 The Chemical Society of Japan.

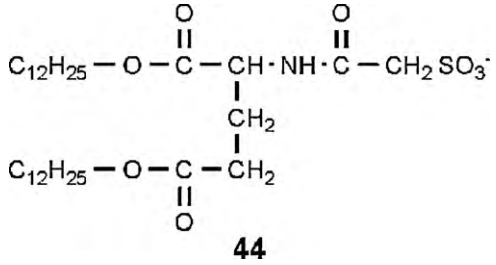

Fig. 41. Chemical structure of lipid counteranion **44**.

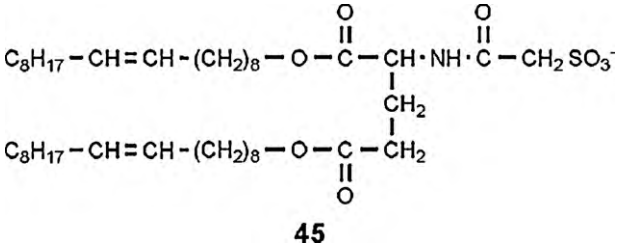

Fig. 43. Chemical structure of lipid counteranions **45**.

ear Pt coordination polymers dissociated into $[Pt(en)_2](\mathbf{36}–\mathbf{43})_2$ and $[PtCl_2(en)_2](\mathbf{36}–\mathbf{43})_2$ at elevated temperatures, but the one-dimensional complexes are reassembled upon cooling (Fig. 40k).

One-dimensional halogen-bridged, mixed valence palladium complexes ($[Pd(en)_2][PdCl_2(en)_2](\mathbf{40})_4$) and heterometallic complexes ($[Pd(en)_2][PtCl_2(en)_2](\mathbf{40})_4$ and $[Ni(en)_2][PtCl_2(en)_2](\mathbf{40})_4$) have also been reported [72]. These complexes had similar behavior to the platinum complexes, and their colors and morphologies can be influenced by external stimuli.

Linear lipophilic $[Pt(en)_2][PtCl_2(en)_2](\mathbf{44})_4$ (Fig. 41) was prepared by another route. Addition of $HAuCl_4$ to $[Pt(en)_2](\mathbf{44})_2$ (colorless) in dichloromethane yielded the intensely colored chloro-bridged mixed-valence complex [73]. In this polymeric complex, the intensity of the CT absorption depends on the amount of tetrachloroaurate(III) added to the reaction. The maximum intensity was obtained at 3:1 $[Pt(en)_2](\mathbf{44})_2/HAuCl_4$. In addition, the ratio also affected the morphology of $[Pt(en)_2][PtCl_2(en)_2](\mathbf{44})_4$ when observed by TEM (Fig. 42). Before the addition of Au(III) ion, $[Pt(en)_2](\mathbf{44})_2$ only gave irregular microcrystalline aggregates (Fig. 42a). Upon adding $HAuCl_4$, nanowires were obtained (Fig. 42b–d), and the most developed nanowires (lengths of 30–100 microns and widths of ca. 670 nm) were observed from the sample of 3:1 $[Pt(en)_2](\mathbf{44})_2/HAuCl_4$ (Fig. 42c). The analogous bromide-bridged structure was prepared with $AuBr_3$ and exhibited similar behavior.

Kimizuka and co-workers have also prepared lipophilic mixed-valence Pt complexes $[Pt(en)_2][PtCl_2(en)_2](\mathbf{45})_4$ (Fig. 43) that self-assemble into two-dimensional honeycombs templated by water droplets condensed from moisture [74]. The TEM image of a sample prepared at 0 °C showed that well-constructed honeycombs could be observed in a wide area (Fig. 44a). The walls of the honeycombs are composed of the linear coordination polymer $[Pt(en)_2][PtCl_2(en)_2](\mathbf{45})_4$. A magnified TEM image revealed that the cavities of the honeycombs were filled with nanofibers that are ca. 20 nm in width (Fig. 44b). The formation of the honeycomb structure is templated by water droplets that condense on the evaporating dichloromethane solution during the sample preparation. A honeycomb structure with improved order was observed for a sample prepared at 21 °C (Fig. 44c). Since solution studies showed that the coordination polymer dissociated into $[Pt(en)_2](\mathbf{45})_2$ and $[PtCl_2(en)_2](\mathbf{45})_2$ at 21 °C, the formation of honeycombs must derive from the re-polymerization of those two components into the linear mixed-valence chains and self-assembly into the supramolecular structure (Fig. 44e). SEM images

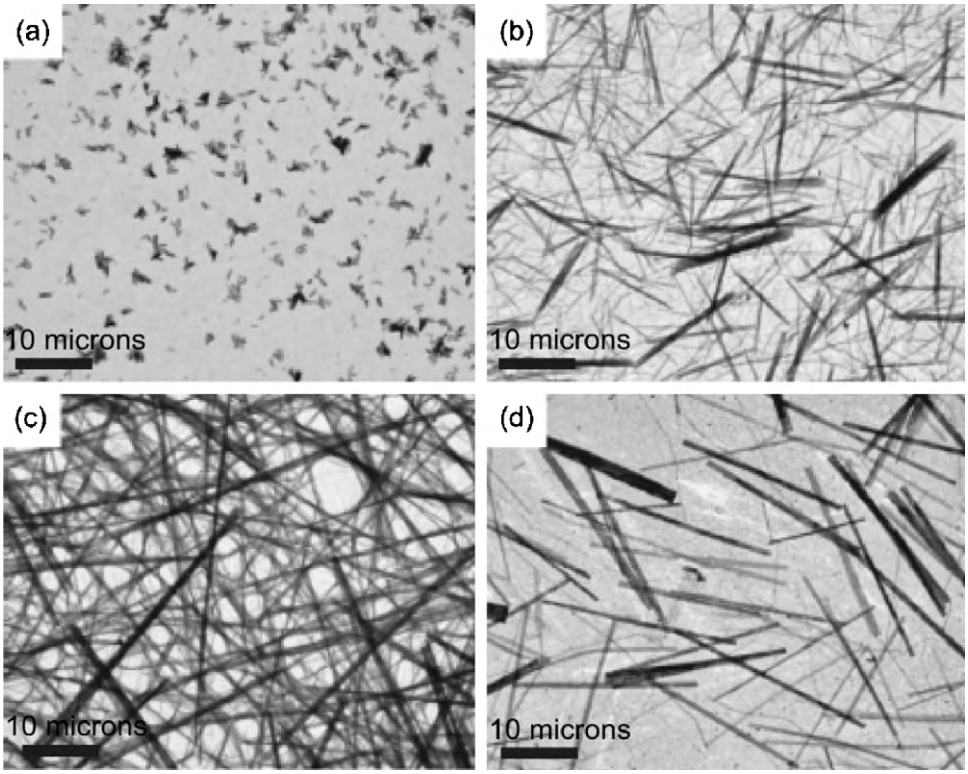

Fig. 42. TEM images of the samples prepared in dichloromethane: (a) $[Pt(en)_2](\mathbf{44})_2$; (b) 6:1, (c) 3:1, and (d) 2:1 of $[Pt(en)_2](\mathbf{44})_2/HAuCl_4$.

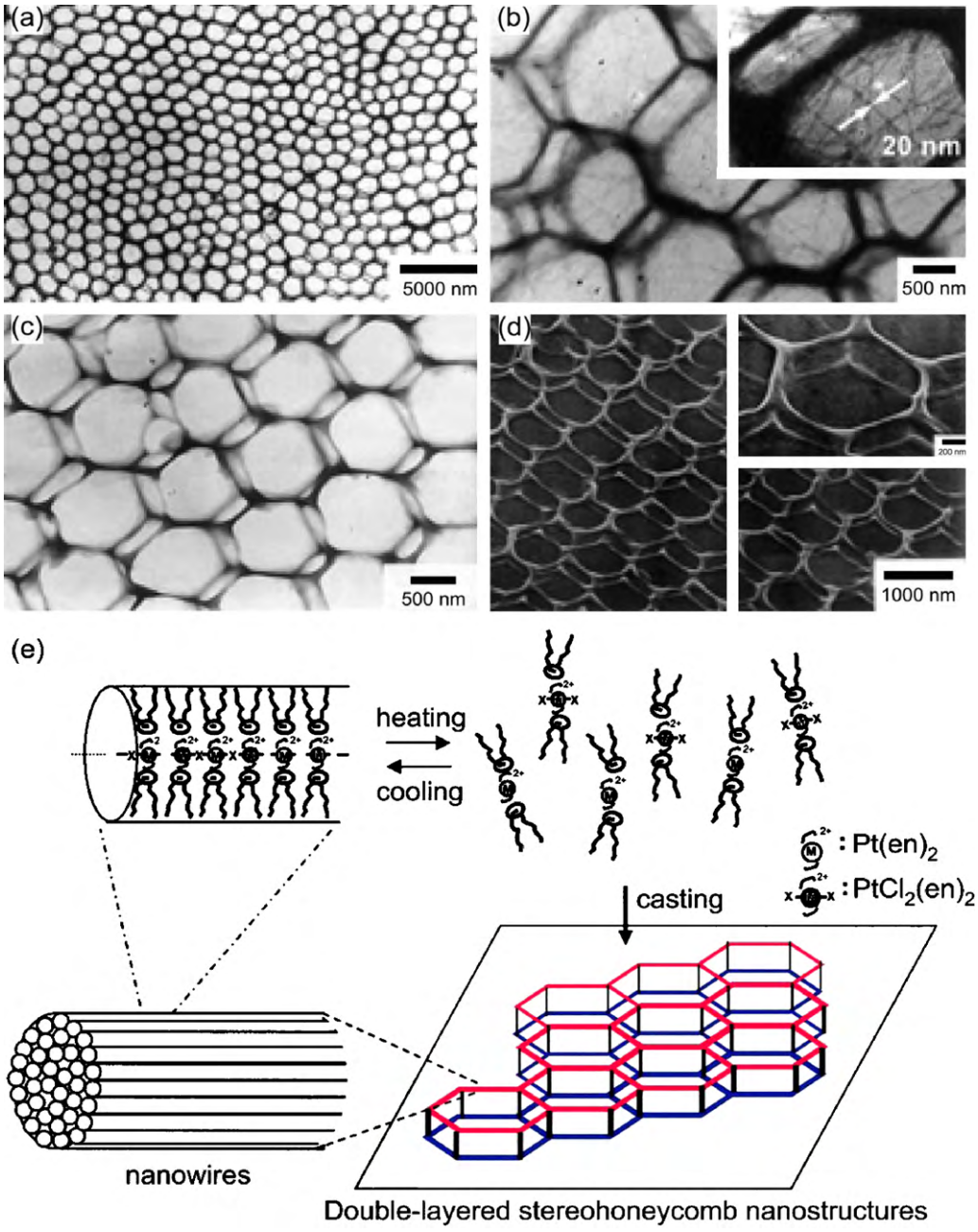

Fig. 44. (a and b) TEM images of $[Pt(en)_2][PtCl_2(en)_2](\mathbf{45})_4$ prepared at 0 °C. (c) TEM and (d) SEM images of the sample prepared at 21 °C. Copyright 2002 National Academy of Sciences, U.S.A. Reproduced with permission from ref. [74].

of the honeycombs clearly showed that the nanostructures are double-layered (Fig. 44d) and the two layers of honeycomb are connected by vertical pillars with heights of ca. 320–370 nm at the corners of the hexagons. The frames (walls and pillars) of the double-layered honeycomb structure are constructed from the hierarchical self-assembly of the lipophilic mixed valence coordination polymer $[Pt(en)_2][PtCl_2(en)_2](\mathbf{45})_4$ (Fig. 44e).

4. Other nanofibers

This review has highlighted several recent examples of metal-containing nanofibers produced using coordination chemistry, where the metal has usually had a central role in the self-assembly. For the sake of completion, we would like to mention several examples of metal-containing nanofibers that have been developed where the metal is not critical to the assembly, but can still be active in the function of the material. Also, we highlight one article that was published while this manuscript was under review. The interested reader is encouraged to examine the original literature for leading references and further details.

Organometallic species have been incorporated into nanofibers by several techniques. Manners and co-workers have been actively developing nanofibers that incorporate metals by the self-assembly of block copolymers where one of the blocks contains a poly(metallocene) component. For example, poly(isoprene)–poly(ferrocenylsilane) block copolymers form long, fibrous micelles that contain metals [75]. Poly(dimethylsiloxane)–poly(ferrocenylsilane) block copolymers also form long fibrous structures with diameters of ca. 25 nm and lengths of >100 μm [76]. These materials have redox-active metal centers that may be used to change the color and properties of the fibers, and they are potential precursors to magnetic nanowires.

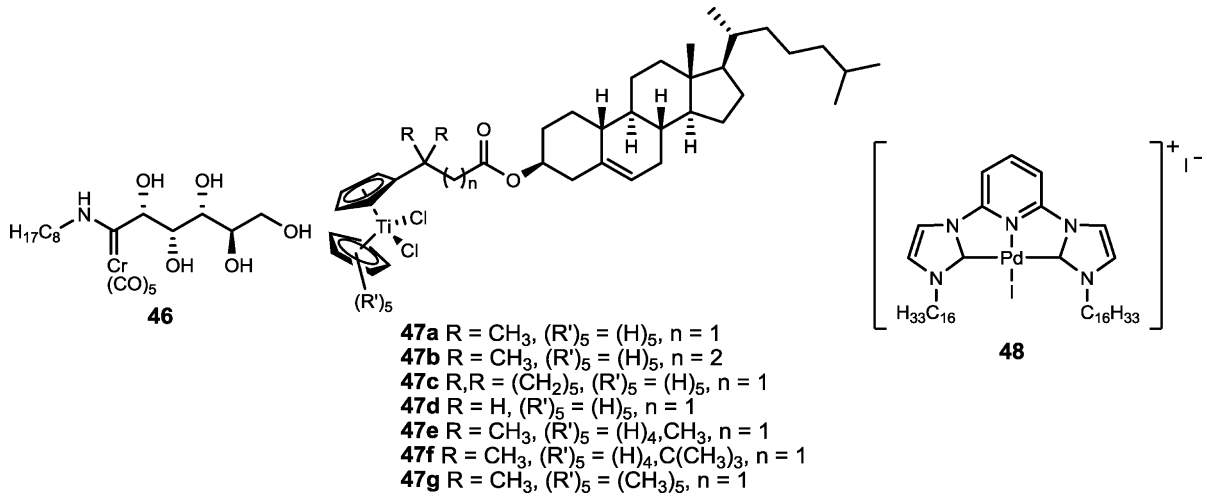

Fig. 45. Chemical structures of low molecular weight metal-containing gelators **46**–**48**.

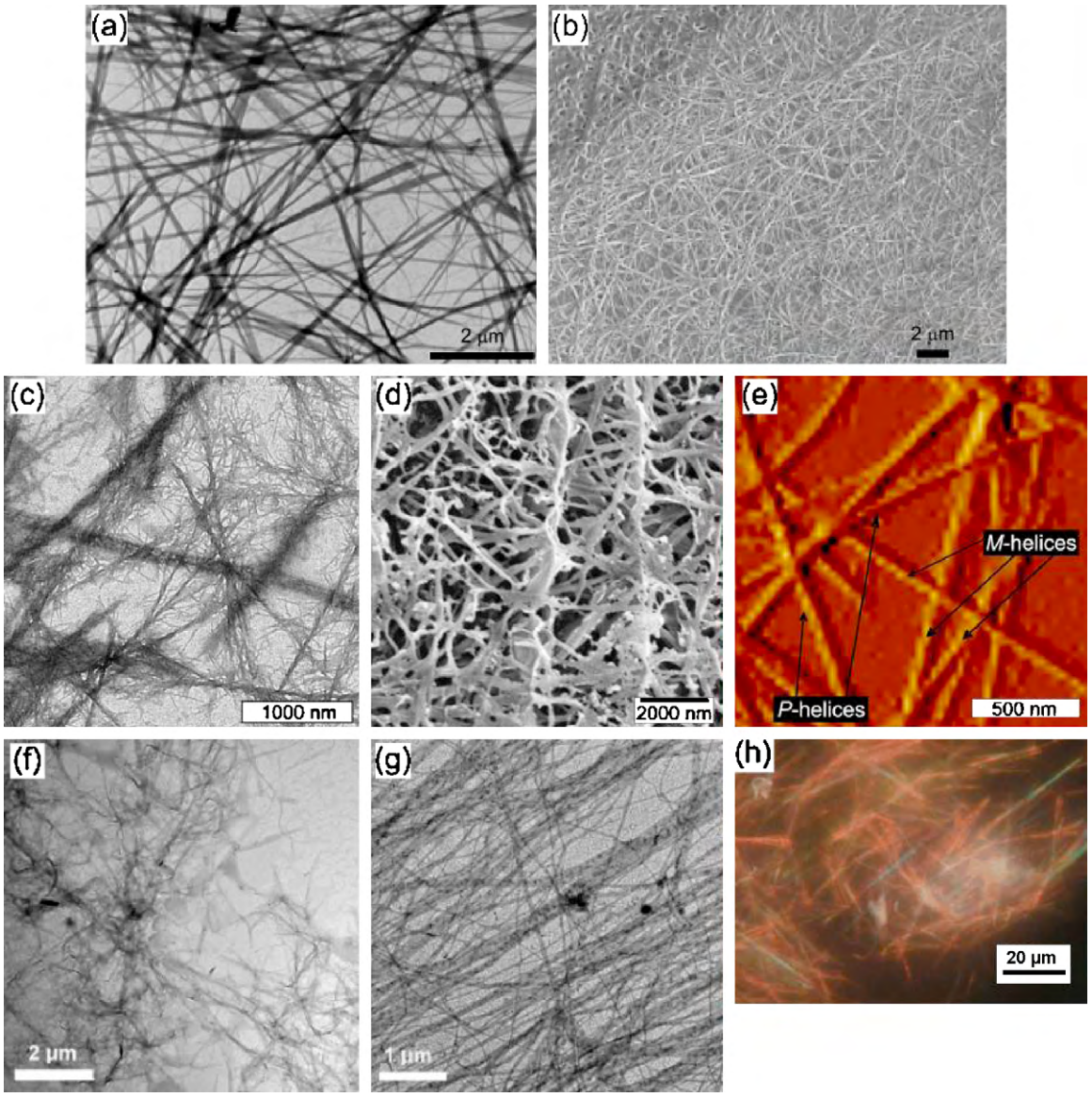

Fig. 46. (a) TEM and (b) SEM images of the gels of complex **46** prepared in chloroform and benzene/chloroform, respectively. Copyright Wiley-VCH Verlag GmbH and Co. KGaA. Reproduced with permission from ref. [77]. (c) TEM, (d) SEM and (e) AFM images of the gel of complex **47a** prepared in toluene. Reprinted with permission from ref. [78b]. Copyright 2009 American Chemical Society. (f and g) TEM images of the gels of complex **48** prepared in DMSO and DMF, respectively. Copyright Wiley-VCH Verlag GmbH and Co. KGaA. Reproduced with permission from ref. [57a]. (h) Dark-field optical microscopic image of the gel of a modified pincer complex in an ionic liquid. Copyright Wiley-VCH Verlag GmbH and Co. KGaA. Reproduced with permission from ref. [79].

Dötz and co-workers have reported several fiber-forming low molecular mass gelators equipped with metal complexes. They first prepared a carbohydrate derivative that functioned as a carbene ligand for $Cr(CO)_5$ (**46**, Fig. 45) [77]. This molecule was found to form stable gels, and high quality fibers were observed by TEM and SEM (Fig. 46a and b). In another study, they reported a series of cholesterol molecules functionalized with titanocene and different substituents (e.g., **47** in Fig. 45) that formed twisted, helical fibers (Fig. 46c–e) [78]. Moreover, they found that incorporation of titanocene enhanced the range of solvents gelated compared with the purely organic analogue where the titanocene is replaced by an aromatic moiety. Pyridine-bridged bis(carbene) palladium pincer complexes (e.g., **48**, Fig. 45) assemble into fibers (Fig. 46f and g) and form gels in several solvents [57a]. Significantly, the authors showed that the organometallic gels are active catalysts for Michael addition reactions. In an extension of this study, they found that the modified pincer complexes could also form fibers (Fig. 46h) and gels in ionic liquids in addition to many organic solvents [79]. The authors invoked π–π interactions, van der Waals interactions, and possibly metal–metal interactions to explain the supramolecular assembly.

While this manuscript was under review, a very interesting paper was published that reports nanofibers from the controlled diffusion of Cu(II) ions into a solution containing NaOH and D- or L-aspartic acid [80]. Extremely long (centimeters), well-defined nanofibers with diameters of 100–200 nm were obtained and imaged by TEM. CD studies confirmed that the fibers are homochiral, though the structure of the fibers is not well known. By varying the metal ion and the amino acid, it is likely that this elegant method can be applied to make a new family of metal-containing nanofibers for potential catalytic and sensing applications.

5. Summary

Metal-containing nanofibers share a common thread: they are fascinating materials with intriguing structures, dynamic properties, and excellent potential for real applications. Numerous researchers have made significant breakthroughs in the understanding of molecular assembly of coordination complexes with the goal of assembling nanofibers. Self-assembly through coordination chemistry and also through electrostatic interactions provides a robust strategy to generate diverse one-dimensional fibrous structures with various degrees of control. This bottom-up approach renders an easy way to tune the properties of the nanofibers by modifying the functionality of the organic building blocks, such as the peripheral substituents and shape of the ligands. In addition, changes in the geometry, oxidation state, magnetic properties, and electronic configuration of the metal centers in the coordination polymers alter the morphology and properties of the fibrous aggregates.

Recent investigations in the field demonstrate the potential of using the sensitivity of metal–ligand interactions to external stimuli to produce changes in structure and properties of fibrillar materials. For example, Kimizuka has unveiled a new coordination-chemistry based approach to controlling the properties of physical gels, and this may open new opportunities for controlled drug delivery, gel-based actuators, and other intriguing applications.

Another interesting area of exploration is the use of coordination chemistry to develop new materials with hierarchical supramolecular structures. While significant advances using hydrogen-bonding have advanced this field, coordination chemistry has been rarely applied. Given the large number and diversity of coordination structures available, it should be possible to construct very interesting, functional hierarchically structured nanofibers.

In spite of the significant advances that have been seen, there are still many areas to explore. Coordination nanofibers with direct metal–metal bonding, nanofibers composed of hydrogen-bonded metal complexes, and nanofibers that are hollow are exciting areas that have received little attention. The development of hollow nanofibers based on coordination chemistry may be useful to generate catalytic and electrocatalytic materials.

Without a doubt, we can expect many new exciting developments to emerge in the field of fibrillar coordination chemistry in the coming decade.

Acknowledgements

We thank UBC and the Natural Sciences and Engineering Research Council (NSERC) of Canada for funding (Discovery Grant and SRO Grant). We are grateful to several co-workers who have undertaken research projects on nanofibers in our laboratory during the past 6 years, especially Amanda Gallant and Richard (Zhen) Yu. Finally, we are indebted to our collaborators who have assisted with electron microscopy, X-ray diffraction, mass spectrometry, AFM, light scattering, and solid-state NMR spectroscopy measurements; many of them are listed as co-authors among the references.

References

[1] G.A. Ozin, Adv. Mater. 4 (1992) 612.
[2] K.S. Chichak, S.J. Cantrill, A.R. Pease, S.-H. Chiu, G.W.V. Cave, J.L. Atwood, J.F. Stoddart, Science 304 (2004) 1308.
[3] B. Hasenknopf, J.-M. Lehn, B.O. Kneisel, G. Baum, D. Fenske, Angew. Chem. Int. Ed. 35 (1996) 1838.
[4] J.J. Michels, M.J. O'Connell, P.N. Taylor, J.S. Wilson, F. Cacialli, H.L. Anderson, Chem. Eur. J. 9 (2003) 6167.
[5] O.M. Yaghi, M. O'Keeffe, N.W. Ockwig, H.K. Chae, M. Eddaoudi, J. Kim, Nature 423 (2003) 705.
[6] (a) P.D. Frischmann, M.J. MacLachlan, Chem. Commun. (2007) 4480;
(b) P.D. Frischmann, A.J. Gallant, J.H. Chong, M.J. MacLachlan, Inorg. Chem. 47 (2008) 101.
[7] (a) C. Tschierske, Nature 419 (2002) 681;
(b) S.D. Peroukidis, A.G. Vanakaras, D.J. Photinos, J. Chem. Phys. 123 (2005) 164904.
[8] (a) O. Ikkala, R.H.A. Ras, N. Houbenov, J. Ruokolainen, M. Pääkkö, J. Laine, M. Leskelä, L.A. Berglund, T. Lindström, G. ten Brinke, H. Iatrou, N. Hadjichristidis, C.F.J. Faul, Faraday Discuss. 143 (2009) 95;
(b) C.C. Lee, C. Grenier, E.W. Meijer, A.P.H.J. Schenning, Chem. Soc. Rev. 38 (2009) 671.
[9] (a) A.P.H.J. Schenning, E.W. Meijer, Chem. Commun. (2005) 3245;
(b) A.P.H.J. Schenning, P. Jonkheijm, F.J.M. Hoeben, J. Van Herrikhuyzen, S.C.J. Meskers, E.W. Meijer, L.M. Herz, C. Daniel, C. Silva, R.T. Phillips, R.H. Friend, D. Beljonne, A. Miura, S. De Feyter, M. Zdanowska, H. Uji-i, F.C. De Schryver, Z. Chen, F. Würthner, M. Mas-Torrent, D. den Boer, M. Durkut, P. Hadley, Syn. Met. 147 (2004) 43;
(c) N. Kimizuka, Adv. Mater. 12 (2000) 1461.
[10] (a) J. Roosma, T. Mes, P. Leclere, A.R.A. Palmans, E.W. Meijer, J. Am. Chem. Soc. 130 (2008) 1120;
(b) M.M.J.F. Koenders, L. Yang, R.G. Wismans, K.O. van der Werf, D.P. Reinhardt, W. Daamen, M.L. Bennink, P.J. Dijkstra, T.H. van Kuppevelt, J. Feijen, Biomaterials 30 (2009) 2425;
(c) C.R. Carlisle, C. Coulais, M. Namboothiry, D.L. Carroll, R.R. Hantgan, M. Guthold, Biomaterials 30 (2009) 1205.
[11] (a) J.D. Hartgerink, E. Beniash, S.I. Stupp, Science 294 (2001) 1684;
(b) Z.-M. Huang, Y.-Z. Zhang, M. Kotaki, S. Ramakrishna, Compos. Sci. Technol. 63 (2003) 2223;
(c) E.-R. Kenawy, F.I. Abdel-Hay, M.H. El-Newehy, G.E. Wnek, Mater. Chem. Phys. 113 (2009) 296.
[12] (a) T.J. Koob, Comp. Biochem. Physiol., Part A: Mol. Integr. Physiol. 133 (2002) 1171;
(b) K. Rajangam, H.A. Behanna, M.J. Hui, X. Han, J.F. Hulvat, J.W. Lomasney, S.I. Stupp, Nano Lett. 6 (2006) 2086;
(c) R.G. Ellis-Behnke, Y.-X. Liang, S.-W. You, D.K.C. Tay, S. Zhang, K.-F. So, G.E. Schneider, Proc. Natl. Acad. Sci. U.S.A. 103 (2006) 5054;
(d) J. Hu, K. Feng, X. Liu, P.X. Ma, Biomaterials 30 (2009) 5061;
(e) H. Yoshimoto, Y.M. Shin, H. Terai, J.P. Vacanti, Biomaterials 24 (2003) 2077;
(f) X. Zong, H. Bien, C.-Y. Chung, L. Yin, D. Fang, B.S. Hsiao, B. Chu, E. Entcheva, Biomaterials 26 (2005) 5330.
[13] (a) J.H. Jung, S. Shinkai, Top. Curr. Chem. 248 (2004) 223;
(b) A. Westcott, C.J. Sumby, R.D. Walshaw, M.J. Hardie, New J. Chem. 33 (2009) 902.

[14] A.R. Hirst, B. Escuder, J.F. Miravet, D.K. Smith, Angew. Chem. Int. Ed. 47 (2008) 8002.
[15] A. Motulsky, M. Lafleur, A.-C. Couffin-Hoarau, D. Hoarau, F. Boury, J.-P. Benoit, J.-C. Leroux, Biomaterials 26 (2005) 6242.
[16] F. Rodríguez-Llansola, B. Escuder, J.F. Miravet, J. Am. Chem. Soc. 131 (2009) 11478.
[17] K. Sugiyasu, N. Fujita, S. Shinkai, J. Mater. Chem. 15 (2005) 2747.
[18] F. Fages, Angew. Chem. Int. Ed. 45 (2006) 1680.
[19] K. Tuzlakoglu, N. Bolgen, A.J. Salgado, M.E. Gomes, E. Piskin, R.L. Reis, J. Mater. Sci. Mater. Med. 16 (2005) 1099.
[20] J. Doshi, D.H. Reneker, J. Electrostat. 35 (1995) 151.
[21] A. Martins, R.L. Reis, N.M. Neves, Int. Mater. Rev. 53 (2008) 257.
[22] D.H. Reneker, I. Chun, Nanotechnology 7 (1996) 216.
[23] D. Li, Y. Xia, Nano Lett. 4 (2004) 933.
[24] (a) J.P. Hill, W. Jin, A. Kosaka, T. Fukushima, H. Ichihara, T. Shimomura, K. Ito, T. Hashizume, N. Ishii, T. Aida, Science 304 (2004) 1481;
(b) J.J.L.M. Cornelissen, M. Fischer, N.A.J.M. Sommeredijk, R.J.M. Nolte, Science 280 (1998) 1427;
(c) J.J.L.M. Cornelissen, J.J.J.M. Donners, R. de Gelder, W.S. Graswinckel, G.A. Metselaar, A.E. Rowan, N.A.J.M. Sommerdijk, R.J.M. Nolte, Science 293 (2001) 676;
(d) F.A. Aldaye, P.K. Lo, P. Karam, C.K. McLaughlin, G. Cosa, H.F. Sleiman, Nat. Nanotech. 4 (2009) 349;
(e) W.-D. Jang, T. Aida, Macromolecules 37 (2004) 7325;
(f) D. González-Rodríguez, J.L.J. van Dongen, M. Lutz, A.L. Spek, A.P.H.J. Schenning, E.W. Meijer, Nat. Chem. 1 (2009) 151.
[25] (a) Y. Yamanoi, Y. Sakamoto, T. Kusukawa, M. Fujita, S. Sakamoto, K. Yamaguchi, J. Am. Chem. Soc. 123 (2001) 980;
(b) B. Hasenknopf, J.-M. Lehn, N. Boumediene, A. Dupont-Gervais, A. Van Dorsselaer, B. Kneisel, D. Fenske, J. Am. Chem. Soc. 119 (1997) 10956;
(c) S. Leininger, B. Olenyuk, P.J. Stang, Chem. Rev. 100 (2000) 853.
[26] (a) O. Kahn, C.J. Martinez, Science 279 (1998) 44;
(b) O. Kahn, Acc. Chem. Res. 33 (2000) 647;
(c) H. Okamoto, M. Yamashita, Bull. Chem. Soc. Jpn. 71 (1998) 2023.
[27] (a) G.W. Gokel, W.M. Leevy, M.E. Weber, Chem. Rev. 104 (2004) 2723;
(b) B. Sarkar, P. Mukhopadhyay, P.K. Bharadwaj, Coord. Chem. Rev. 236 (2003) 1;
(c) E. Rizzarelli, G. Vecchio, Coord. Chem. Rev. 188 (1999) 343.
[28] (a) S.S. Tandon, S.D. Bunge, L.K. Thompson, Chem. Commun. (2007) 798;
(b) M. Thirumavalavan, P. Akilan, M. Kandaswamy, K. Chinnakali, G.S. Kumar, H.K. Fun, Inorg. Chem. 42 (2003) 3308;
(c) W. Huang, S. Gou, D. Hu, S. Chantrapromma, H.-K. Fun, Q. Meng, Inorg. Chem. 40 (2001) 1712.
[29] (a) S.-i. Kawano, S.-i. Tamaru, N. Fujita, S. Shinkai, Chem. Eur. J. 10 (2004) 343;
(b) K. Balakrishnan, A. Datar, W. Zhang, X. Yang, T. Naddo, J. Huang, J. Zuo, M. Yen, J.S. Moore, L. Zang, J. Am. Chem. Soc. 128 (2006) 6576;
(c) K. Nakao, M. Nishimura, T. Tamachi, Y. Kuwatani, H. Miyasaka, T. Nishinaga, M. Iyoda, J. Am. Chem. Soc. 128 (2006) 16740.
[30] A. Tsuda, Bull. Chem. Soc. Jpn. 82 (2009) 11.
[31] (a) D. Gosztola, M.P. Niemczyk, M.R. Wasielewski, J. Am. Chem. Soc. 120 (1998) 5118;
(b) M.U. Winters, E. Dahlstedt, H.E. Blades, C.J. Wilson, M.J. Frampton, H.L. Anderson, B. Albinsson, J. Am. Chem. Soc. 129 (2007) 4291;
(c) A. Huijser, B.M.J.M. Suijkerbuijk, R.J.M. Klein Gebbink, T.J. Savenije, L.D.A. Siebbeles, J. Am. Chem. Soc. 130 (2008) 2485;
(d) G. Steinberg-Yfrach, P.A. Liddell, S.-C. Hung, A.L. Moore, D. Gust, T.A. Moore, Nature 385 (1997) 239;
(e) T.S. Balaban, N. Berova, C.M. Drain, R. Hauschild, X. Huang, H. Kalt, S. Lebedkin, J.-M. Lehn, F. Nifaitis, G. Pescitelli, V.I. Prokhorenko, G. Riedel, G. Smeureanu, J. Zeller, Chem. Eur. J. 13 (2007) 8411.
[32] (a) M. Takeuchi, S. Tanaka, S. Shinkai, Chem. Commun. (2005) 5539;
(b) T. Kishida, N. Fujita, K. Sada, S. Shinkai, Langmuir 21 (2005) 9432;
(c) M. Shirakawa, N. Fujita, S. Shinkai, J. Am. Chem. Soc. 127 (2005) 4164.
[33] (a) T. Kishida, N. Fujita, O. Hirata, S. Shinkai, Org. Biomol. Chem. 4 (2006) 1902;
(b) Y. Guan, S.-H. Yu, M. Antonietti, C. Böttcher, C.F.J. Faul, Chem. Eur. J. 11 (2005) 1305;
(c) G. Lu, X. Zhang, X. Cai, J. Jiang, J. Mater. Chem. 19 (2009) 2417.
[34] (a) G.J.E. Davidson, L.A. Lane, P.R. Raithby, J.E. Warren, C.V. Robinson, J.K.M. Sanders, Inorg. Chem. 47 (2008) 8721;
(b) M. Koepf, J.A. Wytko, J.-P. Bucher, J. Weiss, J. Am. Chem. Soc. 130 (2008) 9994.
[35] Z. Wang, C.J. Medforth, J.A. Shelnutt, J. Am. Chem. Soc. 126 (2004) 15954.
[36] Z. Wang, K.J. HO, C.J. Medforth, J.A. Shelnutt, Adv. Mater. 18 (2006) 2557.
[37] A. Ikeda, M. Ayabe, S. Shinkai, Chem. Lett. 30 (2001) 1138.
[38] (a) G. de la Torre, P. Vázquez, F. Agulló-López, T. Torres, Chem. Rev. 104 (2004) 3723;
(b) R.F. Parton, I.F.J. Vankelecom, M.J.A. Casselman, C.P. Bezoukhanova, J.B. Uytterhoeven, P.A. Jacobs, Nature 370 (1994) 541;
(c) R.J. Mortimer, Electrochim. Acta 44 (1999) 2971;
(d) R. Bonnett, Chem. Soc. Rev. 24 (1995) 19;
(e) S. Dogo, J.-P. Germain, C. Maleysson, A. Pauly, Thin Solid Films 219 (1992) 251.
[39] X. Huang, F. Zhao, Z. Li, Y. Tang, F. Zhang, C.-H. Tung, Langmuir 23 (2007) 5167.
[40] (a) V. Huber, M. Katterle, M. Lysetska, F. Würthner, Angew. Chem. Int. Ed. 44 (2005) 3147;
(b) C. Röger, M.G. Müller, M. Lysetska, Y. Miloslavina, A.R. Holzwarth, F. Würthner, J. Am. Chem. Soc. 128 (2006) 6542;
(c) V. Huber, S. Sengupta, F. Würthner, Chem. Eur. J. 14 (2008) 7791.
[41] K. Adachi, K. Chayama, H. Watarai, Langmuir 22 (2006) 1630.
[42] K. Adachi, K. Chayama, H. Watarai, Chirality 18 (2006) 599.
[43] A. Petitjean, L.A. Cuccia, M. Schmutz, J.-M. Lehn, J. Org. Chem. 73 (2008) 2481.
[44] (a) S. Margadonna, K. Prassides, Y. Iwasa, Y. Taguchi, M.F. Craciun, S. Rogge, A.F. Morpurgo, Inorg. Chem. 45 (2006) 10472;
(b) J.T. Davis, Angew. Chem. Int. Ed. 43 (2004) 668.
[45] (a) J.T. Davis, G.P. Spada, Chem. Soc. Rev. 36 (2007) 296;
(b) S.L. Forman, J.C. Fettinger, S. Pieraccini, G. Gottarelli, J.T. Davis, J. Am. Chem. Soc. 122 (2000) 4060;
(c) A. Wong, R. Ida, L. Spindler, G. Wu, J. Am. Chem. Soc. 127 (2005) 6990.
[46] V. Sidorov, F.W. Kotch, M. El-Kouedi, J.T. Davis, Chem. Commun. (2000) 2369.
[47] L.E. Buerkle, Z. Li, A.M. Jamieson, S.J. Rowan, Langmuir 25 (2009) 8833.
[48] J. Iball, C.H. Morgan, H.R. Wilson, Nature 199 (1963) 688.
[49] M.P.H. Lee, G.N. Parkinson, P. Hazel, S. Neidle, J. Am. Chem. Soc. 129 (2007) 10106.
[50] J.K.-H. Hui, P.D. Frischmann, C.-H. Tso, C.A. Michal, M.J. MacLachlan, Chem. Eur. J. 16 (2010) 2453.
[51] A.J. Gallant, M.J. MacLachlan, Angew. Chem. Int. Ed. 42 (2003) 5307.
[52] (a) S.A. Joshi, N.D. Kulkarni, Chem. Commun. (2009) 2341;
(b) O. Roubeau, A. Colin, V. Schmitt, R. Clérac, Angew. Chem. Int. Ed. 43 (2004) 3283.
[53] X. Zhang, Z.-K. Chen, K.P. Loh, J. Am. Chem. Soc. 131 (2009) 7210.
[54] S. Jung, M. Oh, Angew. Chem. Int. Ed. 47 (2008) 2049.
[55] J.K.-H. Hui, Z. Yu, M.J. MacLachlan, Angew. Chem. Int. Ed. 46 (2007) 7980.
[56] J.K.-H. Hui, Z. Yu, T. Mirfakhrai, M.J. MacLachlan, Chem. Eur. J. 15 (2009) 13456.
[57] (a) T. Tu, W. Assenmacher, H. Peterlik, R. Weisbarth, M. Nieger, K.H. Dötz, Angew. Chem. Int. Ed. 46 (2007) 6368;
(b) J.B. Beck, S.J. Rowan, J. Am. Chem. Soc. 125 (2003) 13922;
(c) S.-i. Kawano, N. Fujita, S. Shinkai, J. Am. Chem. Soc. 126 (2004) 8592.
[58] Y.-R. Liu, L. He, J. Zhang, X. Wang, C.-Y. Su, Chem. Mater. 21 (2009) 557.
[59] S. Zhang, S. Yang, J. Lan, S. Yang, J. You, Chem. Commun. (2008) 6170.
[60] S. Zhang, S. Yang, J. Lan, Y. Tang, Y. Xue, J. You, J. Am. Chem. Soc. 131 (2009) 1689.
[61] W.L. Leong, S.K. Batabyal, S. Kasapis, J.J. Vittal, Chem. Eur. J. 14 (2008) 8822.
[62] S.K. Batabyal, A.M.P. Peedikakkal, S. Ramakrishna, C.H. Sow, J.J. Vittal, Macromol. Rapid Commun. 30 (2009) 1356.
[63] H. Liu, Q. Zhao, Y. Li, Y. Liu, F. Lu, J. Zhuang, S. Wang, L. Jiang, D. Zhu, D. Yu, L. Chi, J. Am. Chem. Soc. 127 (2005) 1120.
[64] (a) H. Kitagawa, N. Onodera, T. Sonoyama, M. Yamamoto, T. Fukawa, T. Mitani, M. Seto, Y. Maeda, J. Am. Chem. Soc. 121 (1999) 10068;
(b) R. Clérac, H. Miyasaka, M. Yamashita, C. Coulon, J. Am. Chem. Soc. 124 (2002) 12837;
(c) H. Kisihida, H. Matsuzaki, H. Okamoto, T. Manabe, M. Yamashita, Y. Taguchi, Y. Tokura, Nature 405 (2000) 929.
[65] K. Kuroiwa, T. Shibata, A. Takada, N. Nemoto, N. Kimizuka, J. Am. Chem. Soc. 126 (2004) 2016.
[66] K. Kuroiwa, N. Kimizuka, Chem. Lett. 37 (2008) 192.
[67] K. Kuroiwa, T. Shibata, S. Sasaki, M. Ohba, A. Takahara, T. Kunitake, N. Kimizuka, J. Polym. Sci., Part A: Polym. Chem. 44 (2006) 5192.
[68] H. Matsukizono, K. Kuroiwa, N. Kimizuka, Chem. Lett. 37 (2008) 446.
[69] S. Kume, K. Kuroiwa, N. Kimizuka, Chem. Commun. (2006) 2442.
[70] H. Matsukizono, K. Kuroiwa, N. Kimizuka, J. Am. Chem. Soc. 130 (2008) 5622.
[71] (a) N. Kimizuka, N. Oda, T. Kunitake, Inorg. Chem. 39 (2000) 2684;
(b) N. Kimizuka, N. Oda, T. Kunitake, Chem. Lett. 27 (1998) 695;
(c) C.-S. Lee, N. Kimizuka, Chem. Lett. 31 (2002) 1252;
(d) N. Kimizuka, Adv. Mater. 12 (2000) 1461.
[72] N. Kimizuka, S.H. Lee, T. Kunitake, Angew. Chem. Int. Ed. 39 (2000) 389.
[73] K. Yasui, N. Kimizuka, Chem. Lett. 34 (2005) 248.
[74] C.-S. Lee, N. Kimizuka, Proc. Natl. Acad. Sci. U.S.A. 99 (2002) 4922.
[75] J.A. Massey, K. Temple, L. Cao, Y. Rharbi, J. Raez, M.A. Winnik, I. Manners, J. Am. Chem. Soc. 122 (2000) 11577.
[76] J. Raez, I. Manners, M.A. Winnik, Langmuir 18 (2002) 7229.
[77] G. Bühler, M.C. Feiters, R.J.M. Nolte, K.H. Dötz, Angew. Chem. Int. Ed. 42 (2003) 2494.
[78] (a) T. Klawonn, A. Gansäuer, I. Winkler, T. Lauterbach, D. Franke, R.J.M. Nolte, M.C. Feiters, H. Börner, J. Hentschel, K.H. Dötz, Chem. Commun. (2007) 1894;
(b) A. Gansäuer, I. Winkler, T. Klawonn, R.J.M. Nolte, M.C. Feiters, H.G. Börner, J. Hentschel, K.H. Dötz, Organometallics 28 (2009) 1377.
[79] T. Tu, X. Bao, W. Assenmacher, H. Peterlik, J. Daniels, K.H. Dötz, Chem. Eur. J. 15 (2009) 1853.
[80] I. Imaz, M. Rubio-Martínez, W.J. Saletra, D.B. Amabilino, D. Maspoch, J. Am. Chem. Soc. 131 (2009) 18222.

Glossary

chlorin: a porphyrin analogue in which the double bond between two β-carbon atoms of a pyrrole has been reduced to a pyrroline. Thus, chlorin is a heterocycle that is comprised of three pyrroles and one pyrroline connected by four methine linkages.

H-aggregates: aggregates in solution that cause a hypsochromic shift (blue shift) in the absorption band compared that of the monomers.

J-aggregates: aggregates in solution that cause a bathochromic shift (red shift) in the absorption band compared that of the monomers.

thixotropic gel: a gel that becomes liquid upon shaking or stirring, but returns to a gel state upon standing.

xerogel: a fibrous, porous network obtained from the removal of the solvent(s) from a gel.